2009

Static high pressure FT-IR spectroscopic studies of TATB

Brian F. Yulga
University of Nevada Las Vegas

STATIC HIGH PRESSURE FT-IR SPECTROSCOPIC STUDIES OF TATB

by

Brian F. Yulga

Bachelor of Science
University of Wisconsin – Stevens Point
2004

A thesis submitted in partial fulfillment
of the requirements for the

Master of Science Degree in Physics
Department of Physics
College of Sciences

Graduate College
University of Nevada, Las Vegas
December 2009

UNLV
UNIVERSITY OF NEVADA LAS VEGAS

THE GRADUATE COLLEGE

We recommend that the thesis prepared under our supervision by

Brian F. Yulga

entitled

Static High Pressure FT-IR Spectroscopic Studies of TATB

be accepted in partial fulfillment of the requirements for the degree of

Master of Science
Physics

Michael Pravica, Committee Chair

Lon Spight, Committee Member

Stephen Lepp, Committee Member

Clemens Heske, Graduate Faculty Representative

Ronald Smith, Ph. D., Vice President for Research and Graduate Studies
and Dean of the Graduate College

December 2009

ABSTRACT

STATIC HIGH PRESSURE FT-IR SPECTROSCOPIC STUDIES OF TATB

by

Brian F. Yulga

Dr. Michael Pravica, Examination Committee Chair
Associate Professor of Physics
University of Nevada, Las Vegas

Static high-pressure experiments utilizing diamond anvil cells (DACs) provide an alternative method to shockwave studies for extracting precise information on the physical and chemical properties of energetic materials. Due to mechanical restraints (e.g. small sample sizes and apertures), synchrotron radiation sources are ideal for probing the structure of materials at the molecular level.

1,3,5-triamino-2,4,6-trinitrobenzene (TATB) is an insensitive (tertiary) high explosive (iHE) useful in military applications. Compared to other conventional iHEs, it is a safer and more stable energetic material. Its unique properties cause it to be of interest in the energetic materials research community.

A series of Fourier-transform infrared experiments were performed on TATB under high pressure conditions (to 35 GPa) at the National Synchrotron Light Source (NSLS). These results demonstrate that there is no strong evidence for a phase transition in TATB in the studied pressure range. The behavior of NH_2 vibrational modes at high pressure suggests that hydrogen bonding is a reason for the increased insensitivity and stability of TATB. Additionally, low intensity features in the vibrational spectra indicate that subtle structural and/or chemical changes warrant further investigation and analysis.

TABLE OF CONTENTS

LIST OF FIGURES

ACKNOWLEDGMENTS

Several members of the UNLV Physics department faculty and students have provided extensive time and effort in contributing to the success of this work. Besides the supporting members of the committee (Dr. Stephen Lepp, Dr. Lon Spight, and Dr. Clemens Heske), Dr. Oliver Tschauner and Dr. David Schiferl have provided valuable insights into the theoretical underpinnings of this project. Ed Romano and Amanda Gordon contributed greatly by assisting in the data collection and analysis. Zak Quine and Ognjen Grubor-Urosevic extended support by providing unique perspectives on data interpretation.

Dr. Zhenxian Liu was most instrumental in lending support for the experimental preparations, data collection, and interpretations. The several experiments contributing to this project would not have been successfully completed without his guidance.

Finally, this work is dedicated to the late Dr. Malcolm Nicol, a true scientist and educator. His genuine interest in the well-being and support of myself and other students will not be forgotten.

Acknowledged Funding and Support Agencies:

All work and travel expenses were supported by the DoD-MURI / US Army RDECOM ACQ CTR Contract W9011NF-05-1-0266 and the DOE DE-FC88-06NA27684 Cooperative Agreements with UNLV.

The U2A beamline is supported by COMPRES, the Consortium for Materials Properties Research in Earth Sciences, under NSF Cooperative Agreement Grant No.EAR01-35554 and the U.S. DOE (CDAC, Contract No. DEFC03-03N00144).

Use of the National Synchrotron Light Source, Brookhaven National Laboratory, was supported by the U.S. Department of Energy, Office of Science, Office of Basic Energy Sciences, under Contract No. DE-AC02-98CH10886.

CHAPTER 1

INTRODUCTION & BACKGROUND

Since the days when early chemists concocted what would later be known as black powder, explosives have been of interest in many areas of scientific research. After World War II, the focus of energetic materials research has largely been on insensitive high explosives (IHEs). As much "in-the-field" knowledge on various low and high explosives had been acquired by that time, it was determined that there were several problems with contemporary energetic materials. While explosives could be formulated for different purposes (such as low explosives for propellants, and high explosives for blasting agents), control of initiation was the primary issue. There have been many mishaps and tragedies due to the unintentional initiation of energetic materials. Modern explosives (especially devices employing nuclear technology) have the capacity to cause greater levels of destruction than in the past. In particular, situations involving the storage or transportation of explosives, airplane crashes or building fires would have more disastrous consequences. Consequently, the search for IHEs became more critical as safety concerns grew.

1,3,5-triamino-2,4,6-trinitrobenzene (TATB; $C_6H_6N_6O_6$, see Fig. 1) was first synthesized in 1888 by Jackson and Wing[1]. It was precipitated from a product of 1,3,5-tribromo- 2,4,6- trinitrobenzene (TBTNB; $C_6Br_3N_3O_6$) and alcoholic ammonia, in pursuit of methods to create hexaminobenzene. At that time its properties as an energetic material were not explored, which in retrospect was likely due to its high insensitivity (TATB would not have been initiated under laboratory conditions). It was not until the 1950s that interest in heat and shock resistive materials for space applications would lead to renewed investigations on TATB.

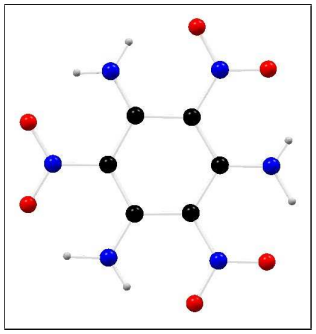

Figure 1: TATB molecule

TATB was first synthesized in significant quantities in the early 1960s, and further investigations in characterization began at Los Alamos Scientific Laboratory and Lawrence Livermore Laboratory (as named at the time; now LANL and LLNL, respectively) for its use in nuclear weapons. It was also recognized that techniques for synthesis affected the purity and particle size. This is one reason that similar plastic bonded explosives (PBXs) containing TATB, developed at different laboratories, exhibit slightly different properties (for example LLNL's LX-17 and LANL's PBX-9502).

Although the synthesis of TATB was expensive (current progress at LLNL shows the promise of cheaper methods, the experimental yield was close to the theoretical maximum density (TMD), and the bulk material had the capability to be easily shaped[2]. Though TATB had a lesser explosive yield than other conventional explosives such as RDX and HMX, the ability to safely machine shaped charges was more critical in nuclear weapon designs. Shown in Tables 1 through 3 on page 11 are some physical properties of TATB, compared to other conventional energetic materials.

Macroscopically, TATB is a yellowish-brown powder, and carefully grown single crystals appear as thin hexagonal prisms. While the molecular symmetry suggests a six-fold rotation symmetry about the planar molecule, the crystallographic symmetry is centrosymmetric, space group $P\bar{1}$, Z = 2[3] (See Figs. 2 and 3). The yellow color is likely explained by the existence of an electronic absorption band in the near-visible to the ultraviolet region. Since light in the blue part of the visible spectrum is absorbed by the sample, the remaining visible light that is not absorbed gives the material a yellowish hue. Since this absorption band has some overlap with blue (488 nm) and green (514 nm or 532 nm) light, this band can be populated by visible light. As a result, lasers used in Raman spectroscopy tend to damage the sample because the high intensity light quickly populates the absorption band. When the absorption bands are highly populated relative to the ground state, molecular bonds have a higher probability of destabilizing. With the laser light inducing chemical changes in the sample, it is difficult to obtain useful Raman spectra of TATB[4].

TATB has been proven to be a successful secondary (or tertiary) explosive material, but current research efforts seek characterization at the molecular level and better understanding of its limits of stability and material properties under extreme conditions. Advances in experimental measurement techniques, combined with more sophisticated and faster computer modeling, allow the potential for a more satisfying explanation for the behavior of TATB. The field of energetic materials research still has many unanswered questions; an understanding of what makes TATB more insensitive compared to other explosives will lead to better design and synthesis of explosives.

Techniques such as x-ray diffraction, Brillouin scattering, and vibrational spectroscopy provide key information on the crystallographic and molecular structure of these materials. Additionally,

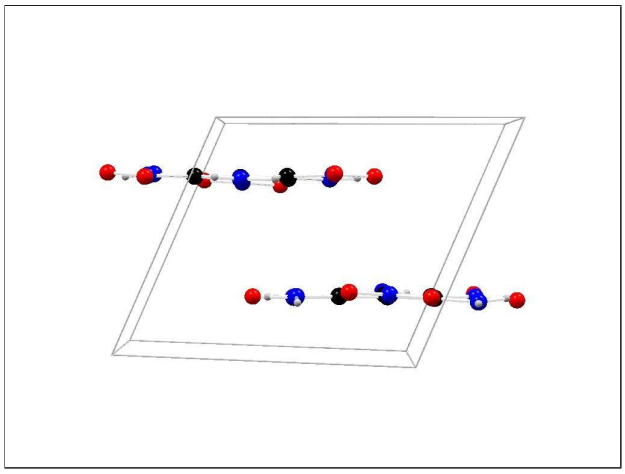

Figure 2: TATB unit cell, perpendicular to z-axis

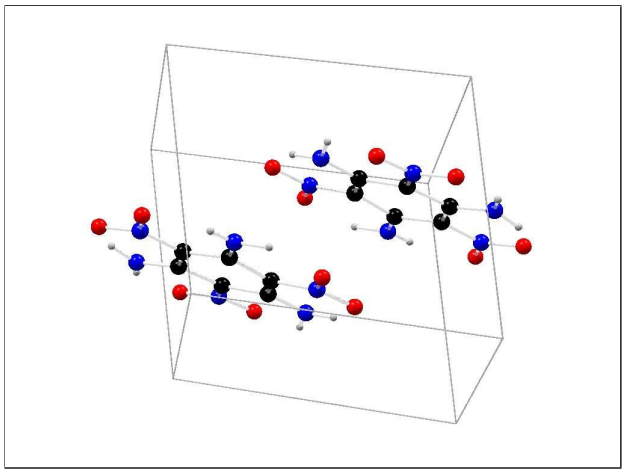

Figure 3: TATB unit cell, along combination of axes

high pressure research on energetic materials attempts to simulate, in a controlled environment, the deflagration or detonation reaction of a "real-world" situation. By measuring various thermodynamic and kinetic parameters, better theories for the fundamental mechanisms of initiation can be formulated[5, 2]. For example, the current understanding of initiation based on "hot spots" does not establish an exact definition of a "hot spot"[6]. Subjecting explosives to the extreme (yet controlled) conditions of static or dynamic high pressure allows determination of both the physical properties of pure systems and also deviations from standard behavior due to impurities or other fluctuations.

High Pressure Research

High pressure experiments may be categorized as either static or dynamic. In dynamic experiments, samples are studied as a shockwave impacts the material. The conditions of shock compression have been studied thoroughly[5], and as a result there are accurate and precise data on the thermodynamic pressure of the material under shock conditions. However, as the Hugoniot state (shocked state) of a material is neither isothermal or adiabatic, there is no direct measurement of the temperature. While shockwave experiments more accurately simulate the conditions of an explosive's initiation, it is currently not possible to achieve an understanding of the initiation/detonation of materials strictly from "first-principles". Consequently, various assumptions, models, and "rules of thumb" are applied in efforts to extrapolate a more complete description of the system. These assumptions extend the usefulness of shockwave data but are ultimately limited in achieving a fundamental understanding of these physical processes.

Complementing dynamic experiments, samples in static high pressure experiments are placed in a containment vessel, and pressure is gradually applied to one or more axes. If the sample is surrounded by a fluid in the vessel, the stress on all axes is identical and there is zero deviatoric stress. In the ideal situation, the pressure may be measured directly by dead-weight experiments. At the high pressures obtained under detonation conditions, there is no direct measurement of the pressure inside the sample chamber, but the temperature is known. Controlling pressure along with external heating or cooling of the high pressure cell is used to probe the phase diagram associated with the thermodynamic Gibb's potential[7]. The thermodynamic condition in a static high pressure experiment is isothermal, and hence can directly measure the main unknown thermodynamic variable in dynamic high pressure experiments.

Static High Pressure Experimentation

The experimental high pressure laboratories within UNLV's High Pressure Science and Engineering Center (HiPSEC) are focused on static diamond anvil cell (DAC) work. Experiments prepared and/or conducted in HiPSEC's facilities range from moderately high pressures (1 to 10 GPa) to pressures exceeding 100 GPa. They can also be conducted at variable temperatures from 11 K all the way up to 1000 K. A variety of DAC designs are available within this pressure regime, and the DAC selected for these experiments allows fine compression adjustments under 50 GPa. Details of this design are shown in the subsequent sections.

Shown below (Fig. 4) is a schematic representation of a diamond anvil cell. The theoretical basis

for the design originates with Bridgman's experiments in the 1950's. Indeed, the current versions of the DAC are not significantly different from the original design in concept; the last several decades have given rise to technological improvements allowing better machining and aligning of parts. As a result, the success of a high pressure DAC experiment depends strongly on the desired range to be studied and the equipment used. While poor science is not being suggested here, it is possible to conduct an experiment with a high-quality DAC carelessly at pressures under 10 GPa and achieve results better than Bridgman.

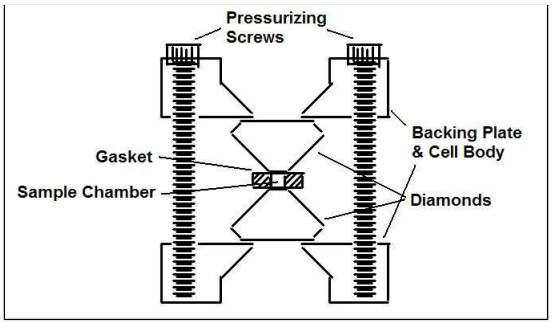

Figure 4: DAC schematic

All DAC designs share some common characteristics: two anvils to apply static compression along an axis, a housing to maintain the latitudinal and longitudinal position and alignment of the anvils, screws or bolts to control the applied force on the housing, and a gasket to confine the sample between the anvils. For many experiments, the choice to use diamond as the anvil is not solely due to its hardness, but also its optically transparent property. When diamonds are not available or when sample spectral features overlap with diamond lines, sapphire and moissonite can be used for lower pressure experiments. In any case, the anvil's position on a backing plate with a conical rear opening allows for ease of sample preparation and measurement (Fig. 4). In particular, the traditional difficulty associated with the DAC in x-ray scattering/diffraction experiments has been due to the small angled aperture reducing the ability to obtain full diffraction information. Newer DAC designs provide apertures in excess of 100 degrees, although the refraction of light through the diamonds reduces the true angular range.

The confining gasket material is usually a somewhat ductile metal, with a hole drilled in the center after having been pre-compressed to form an indentation. For holes smaller than 300 microns, it is usually drilled using electric discharge machining methods. As the gasket material flows out-

wards along the diamond facets with applied force, the seal between the diamonds and the gasket hole rim improves, further stabilizing and pressurizing the sample chamber. Besides the sample and a pressure probe (such as ruby), the sample chamber is filled with a pressure-transmitting medium. This is especially critical for studying materials that are initially solid at room (standard) temperature and pressure (STP). As pressure is applied along the axis of the anvils, only the gasket and pressure-transmitting medium can prevent the sample from being crushed. Additionally, a good pressure-transmitting medium is less susceptible to deviatoric stress and provides a quasi-hydrostatic condition in the sample chamber. From basic physical science, it is analogous to an object near the bottom of a swimming pool. Assuming the object is small, so that gravitational potential differences are negligible, the surrounding water applies equal force per unit area to all sides of the object. Indeed, this is fundamental property of a fluid; any pressure gradients will cause flow until equilibrium (hydrostaticity) is reached. Unfortunately few materials remain in liquid form above 1 GPa at room temperature, so the choice of pressure medium tends toward a pragmatic attempt at finding materials that while solid at high pressure have liquid-like properties.

Determining Pressure Indirectly: Ruby as a Pressure Sensor

Pressures above 2.5 GPa cannot be measured directly by dead-weight piston cylinder (Force / Area) methods[8]. Thus, the determination of pressure in the contemporary DACs used for these experiments must be made by indirect "sensing" methods. Consequently, any probe used must be calibrated, and any intrinsic error in the calibration will propagate to the pressure scale.

While many sensors exist for high pressure measurements, the most common pressure sensor used in optical spectroscopic studies in a DAC at room temperature utilizes the ruby R1 fluorescence wavelength. The popularity of ruby as a pressure probe is largely due to the following: The R1 fluorescence wavelength varies nearly linearly (up to 20 GPa) with respect to pressure enough to allow for the detection of small pressure changes. Additionally, the variation of the fluorescence line is smooth across a relatively large pressure range, allowing the calibration curve to be adequate for a variety of experiments. For the scientist on a limited budget, rubies are inexpensive and readily available. Finally, lasers are now cheap and ubiquitous sources to excite the ruby fluorescence.

Ruby is the common name of aluminum sesquioxide (Al_2O_3) doped with chromium. The α-Al_2O_3 structure is also known as corundum, where the trigonal lattice can be visualized as an array of octahedra. The oxygen atoms sit at the corners of the octahedron, and one aluminum ion at the center. In the case of ruby, the chromium atoms replace a small portion (on the order of one percent or less) of aluminum atoms at their lattice sites, which is known as substitutional doping.

The red fluorescence of ruby is caused by the combination of three properties of ruby: spin-orbit coupling between the chromium ion and the electrostatic crystal field of the octahedral lattice; the distorted shape of the octahedral lattice (a property of corundum); and the electron d-states of chromium. Exciting the ground state of ruby with laser light (usually in the green or blue) pumps electrons to higher states of the $3d^3$ orbitals. Phonon assisted relaxations from the higher electronic excited states transition quickly to the $2E$ state. The delay in relaxation from the $2E$ state to the ground state (caused by the transition being "forbidden") is responsible for the observed fluorescence effect. As the $2E$ state is a reflection of the underlying cubic symmetry, the trigonal symmetry of corundum caused an energy level splitting. As a result, the fluorescence effect is observed to have two slightly different frequencies, corresponding to the R1 and R2 fluorescence lines.

Historically, the R1 line calibration is primarily used for pressure determination. More recent investigations have determined the usefulness of the R2 line pressure dependency. The R2 line is much weaker in intensity, but with decent spectroscopic equipment capable of an accurate measurement, the advantage is clear: Unlike the R1 line, the R2 line exhibits no deviatoric stress dependency.

If a single crystal of ruby is oriented along its c-axis, and stress is applied along this axis (uniaxial compression), the R1 line pressure versus wavelength curve will be different than if compression is along the a-axis. Symmetrical invariance of the R2 line results in identical curves (orientation independence). (For an example of the apparent widening of the R1 line and invariance of the R2 line, see ahead to Figs. 20 and 21). When its measurement is available, this allows the R2 line to be useful in situations where the ruby crystal has intrinsic stress or the conditions in the sample chamber are less than ideal (non-hydrostatic conditions).

Infrared and Raman Vibrational Spectroscopy

An exhaustive description of various physical properties measurements on samples in DACs is beyond the scope of this experiment[8], but it is advantageous to understand the context for which the experiments of this project have been conducted. UNLV's HiPSEC laboratories are primarily equipped to conduct experiments of structural determination using x-ray diffraction and optical molecular spectroscopy (electronic absorption spectroscopy and vibrational spectroscopy).

Single crystal x-ray diffraction techniques provide the most comprehensive and precise structural (mechanical) data on materials. The disadvantage of these methods is that equipment and sample preparation are highly time consuming, and consequently not economical for some inves-

tigations. Optical spectroscopic techniques allow for a more rapid method to obtain basic physical information on many materials (e.g. detection of phase transitions). A higher level of analysis, incorporating density-functional theory (DFT) and group theoretical methods, can be tedious for systems of low symmetry. Consequently, deriving exact structural parameters (such as unit cell dimensions and atomic positions) accurately for these systems is difficult. Without additional experiments employing other techniques, the results of a detailed analysis are highly interpretive.

To qualify the (justified) skepticism of interpretation, it is worthwhile to note that optical spectroscopy is highly useful for identifying interesting problems or effects. For example, since the structure factor of hydrogen is of very low intensity, x-ray diffraction is essentially unable to measure hydrogen bonding in materials. Also, vibrational modes tend to be highly sensitive to phase changes. Static high pressure experiments within HIPSEC that employ these techniques are useful in providing initial information to be used later in single crystal or powder x-ray diffraction experiments. Additionally, systems studied with x-ray powder diffraction can potentially have ambiguous results that can be resolved relatively quickly with vibrational spectroscopy.

Vibrational spectroscopic data may be acquired through two rather different but complementary experimental techniques. Raman spectroscopy utilizes an incident beam of light with a narrow frequency bandwidth to interact with the polarization tensor. Light of an initial frequency ω_0 (usually visible laser light) is inelastically scattered, resulting in a new frequency ω_1. The energy difference $\Delta E = \hbar|\omega_1 - \omega_0|$ corresponds to the energy required to excite the given mode from n to $n + 1$. Because the probability of the Raman effect for an incident photon is low (on the order of 10^{-7}), relatively high-intensity laser light and sensitive detecting equipment must be used. Data acquisition times for high resolution scans over larger frequency ranges can be several hours long. This can be problematic for samples that are photo-sensitive or are heated by the laser light.

Compared to Raman vibrational spectroscopy, infrared (IR) spectroscopy is a more direct probing of vibrational modes. The incident light is of a wide bandwidth, exciting vibrational transitions within the far- to near-infrared spectral range. Whereas the Raman effect excites molecular vibrations that cause a change in the polarization tensor, incident infrared radiation excites molecular vibrations that change the dipole moment. In other words, incident photons are of an energy exactly equal to that required for a vibrational excitation, and the intensity difference between incident light (i.e. reference spectrum) and transmitted light is a measure of the infrared absorption profile[9].

Fourier Transform Infrared (FT-IR) Spectroscopy

Due to various advantages in optical instrumentation and reduced data acquisition times, conventional IR spectrometers are typically Fourier transform (FT) interferometers. Rather than using a monochromator and moving diffraction grating to sweep across a spectral range, FT-IR spectrometers have a Michelson interferometer geometry, with one fixed and one movable mirror. As the mirror is translated across a spatial range, the detector measures the light intensity. The resulting function of intensity versus mirror position (an interferogram) serves as the raw data. To accumulate better statistics, one measurement usually consists of an average of many sweeps of the mirror.

Mathematically, the interferogram is considered as a convolution of all weighted frequencies of light transmitted through the sample (or the spectral distribution of the light source when no sample is present). Deconvoluting this function of intensity versus spatial position ($I(x)$) to intensity versus spatial frequency ($I'(\nu)$) is accomplished with a forward Fourier transformation:

$$I'(\nu) = \int_{-\infty}^{+\infty} I(x) e^{-i\nu x} dx \tag{1.1}$$

Unfortunately, physical data is never a continuum, so applying this function requires an adjustment for discrete values and finite limits of x (mirror position). The associated function for finite data sets is called a discrete Fourier transform (DFT). As the discrete transform is exact only for infinitely large data sets and computational time, various algorithms have been developed to elucidate precise (in the limit of resolution) DFTs with reasonable computational power. Collectively these efficient algorithms are known as fast discrete Fourier transforms (FDFT), and conventionally shortened to FFT. Commercial FT-IR spectrometers tend to be packaged with several FFT routines, the choice of which is used ultimately depends on the user/technician. The Fourier transform is not a uniquely defined function, and hence there are several associated constants to be calibrated (such as amplitude scaling and phase correction).

Synchrotron Radiation Sources for FT-IR Spectroscopy at High Pressure

Conventional Globar sources are generally inadequate for IR spectroscopy through a DAC. Standard diamonds used in DACs are not optically transparent enough in the infrared region to achieve adequate signal-to-noise. Type IIa diamonds, characterized by ultra-low levels of nitrogen impurities, have reduced absorbance in portions of the IR region. While it improves the ability to detect modes in the mid-IR region, Globar sources are still the limiting factor in detecting vi-

brational modes of lower intensity. Synchrotron sources that were designed to accommodate the lower energy far-IR to VUV region (compared to x-ray radiation) provide ideal sources for FT-IR measurements in a DAC.

Through the collaboration of HIPSEC with the U2A beamline of the National Synchrotron Light Source (NSLS) at Brookhaven National Laboratory (BNL), high quality FT-IR data on materials in DACs can be obtained in sometimes limited beamtime (one or two days). The U2A beamline provides the equipment to measure FT-IR in a DAC with a frequency range of 10 cm^{-1} to 10,000 cm^{-1} and a spatial resolution as small as 5×5 μm. Additionally, a cryostat and external heater are available for variable-temperature, high pressure experimentation.

Due to the varied response efficiency of detectors in this wide frequency range, U2A's experimental table is arranged for two optical paths. After the synchrotron source IR radiation travels through the interferometer, the light travels through one of the two paths, through the sample to a mercury:cadmium telluride (MCT) detector for mid-IR experiments, or to a bolometer for far-IR experiments. MCT detectors work on the general principle of the photoelectric effect, while bolometers are more sensitive to lower-energy (far-IR) radiation, detecting by thermal response.

Design of Experiment

As TATB is of interest in the energetic materials research community, and the infrared spectrum of TATB had not been studied to very high pressures [cite: Satija [4]], it was determined that it would be worthwhile to perform a series of FT-IR experiments on TATB under static high pressure conditions. The main goal was to witness any possible phase transitions, with a secondary goal to verify the study by Satija with the complementary technique of infrared spectroscopy.

Table 1: TATB Chemical and Physical Data

Explosive	Type [organic]	Oxygen Balance	Molecular Weight, (g/mol)	Color
TNT	Aromatic monocyclic monosubstituted TNB	-73.9%	227.134	Light yellow
TATB	Aromatic monocyclic polysubstituted TNB	-55%	258.156	Bright yellow
PETN	Open chain aliphatic nitrate ester	-10%	316.146	Clear (white)
RDX	Cycloaliphatic	-21.6%	222.126	Clear (white)

Table 2: TATB Chemical and Physical Data (cont.)

Explosive	Crystal Density theoretical max (g/cc)	Melting point (°C)	Detonation velocity (km/sec), at density	Detonation Pressure [CJ] (GPa)	Heat of Formation (Kcal/g-mol)	Heat of Detonation (Kcal/g-mol)
TNT	1.654	80.8	6.90 @ 1.60	18	-16	247.5
TATB	1.94	350	7.35 @ 1.80	28.9	-36.85	238.2
PETN	1.76	141.3	8.40 @ 1.7	33.7	-128.7	471.1
RDX	1.82	204	8.75 @ 1.76	33.4	14.71	335.4

Table 3: Common TATB PBX formulations

Formulation	% TATB	Remaining constituents	Color
PBX-9502	95	Kel-F 800, 5%	Yellow
LX-17-0	92.5	Kel-F 800, 7.5%	Yellow
PBX-9503	80	HMX, 15%; Kel-F 800, 5%	Purple

CHAPTER 2

EXPERIMENTAL PROCEDURES

Before describing the details of experimental preparation and data collection, it must be noted that this study consists of five individual experiments (separate sample loadings) conducted at beamline U2A of the NSLS. Table 4 designates these experiments.

Where appropriate, the description will note differences in procedure of the experiments. Otherwise, references to "experiment" and "sample" indicate identical procedures for each of the five experiments.

Preparation

TATB samples were prepared in a symmetric-type diamond anvil cell (DAC). Experiments utilized both HIPSEC-owned Syntek (show URL ref http://www.syntek.co.jp/kouatu2.html [10]) and U2A-owned Princeton (CIW) DACs. A disassembled DAC is shown in Figs. 15 and 6. Fig. 5 includes a nickel to indicate the size of a DAC, and Fig. 6 shows the diamond mounted inside the "piston" side of the DAC, and a pre-indented gasket (7 o'clock position).

300 micron culet type IIa diamonds were selected for these experiments. Type IIa diamonds, which have fewer nitrogen impurities, can be distinguished by a lack of electrical conductivity and low absorption in the desired infrared frequency range (internet ref http://www.gemguide.com/news/archives1.htm). A transmission spectra of the diamonds procured from D'Anvils for use within UNLV HIPSEC is shown in Fig. 7.

The frequency range of 1900 – 2500 cm^{-1} shows strong absorption primarily due to water. The complementary nature of Raman spectroscopy allows an alternative method to study this frequency range.

The diamonds were mounted onto the backing plate of the DAC with Stycast® epoxy #[look

Table 4: Experiment Designations

Experiment Designation	Starting Date	Data Collection Region (cm^{-1})	Pressure Range
1	10 Mar. 2006	Mid-IR (700 — 3500)	0 — 12 GPa
2	10 Mar. 2006	Far-IR (100 — 700)	0 — 10 GPa
3	9 Oct. 2007	Mid-IR (700 — 3500)	0 — 11 GPa
4	10 Oct. 2007	Mid-IR (700 — 3500)	0 — 39 GPa
5	11 Oct. 2007	Far-IR (100 — 700)	0 — 30 GPa

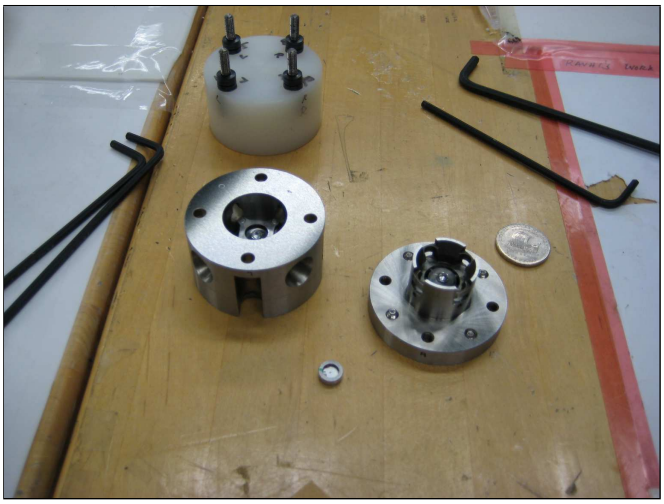

Figure 5: Disassembled DAC, all parts

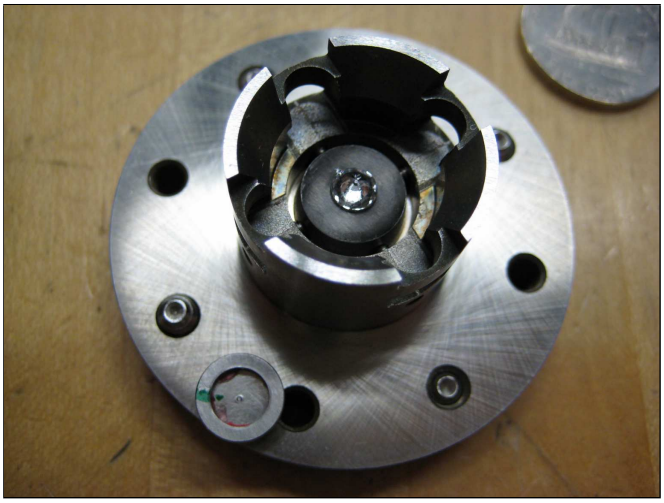

Figure 6: Disassembled DAC, close-up of one anvil

up], which was allowed to cure overnight at room temperature. Then, the diamond culets were aligned to be centered with respect to each other (translational adjustment) and parallel to each other (tilt correction) as best as possible. The symmetric-type DAC retained alignment within machined tolerances throughout the experiments.

Stainless steel (304-hardened) was selected as the gasket material for all experiments. Prior to pre-indentation, the thickness of the gasket was 250 microns, with a diameter of $\frac{1}{4}$ inch. All gaskets used for the experiments were pre-indented to between 30 and 50 microns thick. The sample chamber was drilled with an electric discharge machine (EDM; Hylozoic Products, Seattle, Washington)

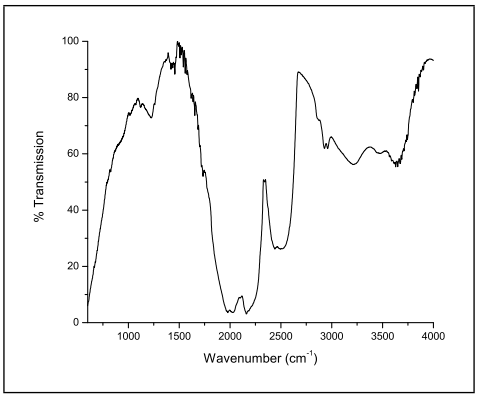

Figure 7: Transmission spectrum through a type IIa diamondwhatever

available in the sample preparation lab for the NSLS X17A beamline. Tungsten wire of thickness between 100 and 130 μm was used as an electrode to achieve the desired sample chamber diameter. Ethanol was used as the dielectric medium (instead of oil), and care was taken to maintain the orientation of the gasket with respect to the diamonds while loading the sample. The EDM is pictured in Figs. 8 and 9.

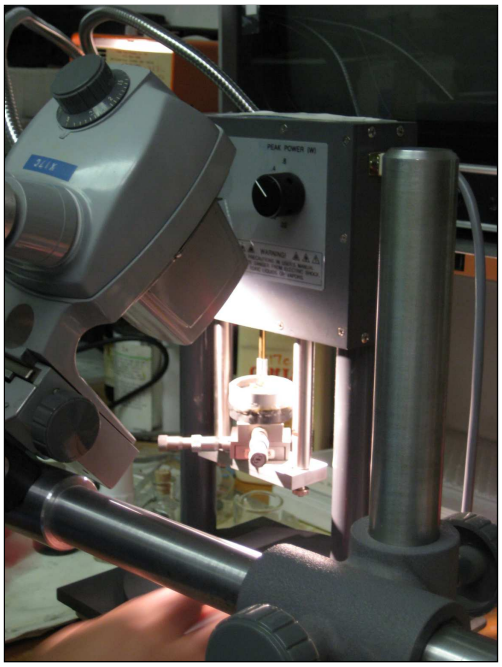

Figure 8: EDM, showing alignment stereo microscope

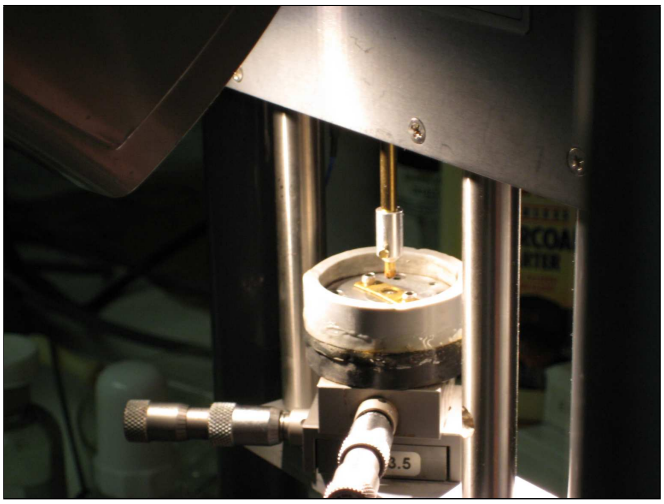

Figure 9: EDM, close-up of stage

Prior to loading sample in the gasket of the DAC, the appropriate sample thickness was determined. This was done by placing TATB powder (ref, Moore LANL batch # for source **??**) on one diamond culet (no gasket) and carefully closing the DAC with the opposing side. A rough check for sample signal saturation was then performed in the synchrotron IR beam. Figs. 10 and 11 show the sample illuminated from below with visible light, and the transmittance through the sample on the data collection computer.

Fig. 10 indicates a condition of moderately good absorption. If too much sample is present, the transmission spectra (red line in Fig. 11) will show peaks that flat-line with the baseline. This can be corrected by carefully bringing the two sides of the DAC together and then slowly rotating and pressing the culets relative to each other. Sample will then flatten and compactify by transfer outwards across the culet and flatten. The transmission is then rechecked and the procedure repeated until no saturation is witnessed. In the other extreme, the profile of Fig. 11 will look nearly identical to Fig. 7 (above, sample diamond transmission). All mid-IR spectra displayed a similar absorption profile, although experiment #5 entailing far-IR measurement intentionally was loaded with extra sample. This caused saturation of the strongest peak, but allowed enhancement of minor peaks. Sample thickness varied between 2 and 10 microns throughout the experiments, with the far-IR measurements requiring thicker samples due to reduced absorption of weaker vibrational modes.

After the sample thickness was determined, the experimental procedure deviated for far-IR and mid-IR measurements. For the mid-IR experiments, half of the sample is scraped away from one culet, and KBr powder is loaded onto the other diamond. When the DAC is reassembled, the

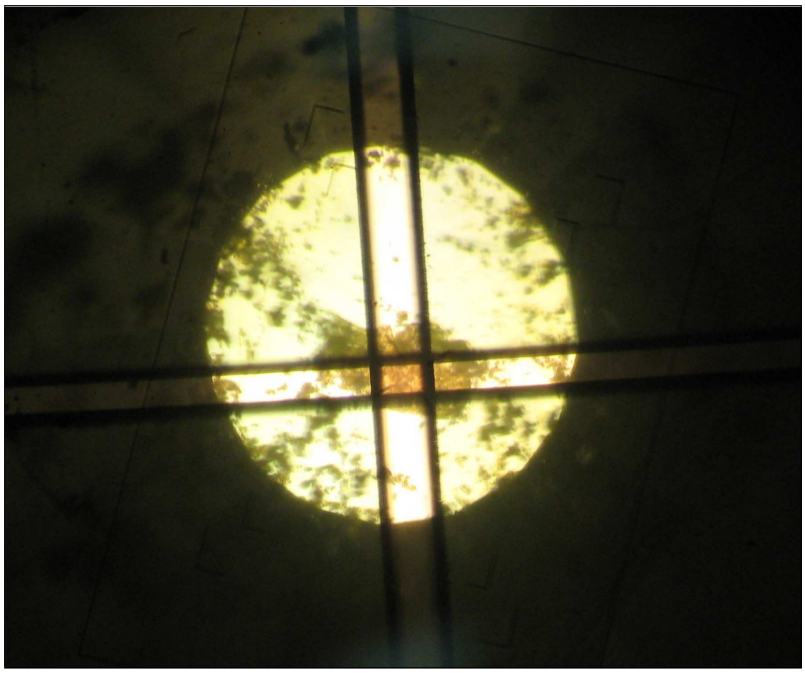

Figure 10: TATB powder on diamond culet, through microscope

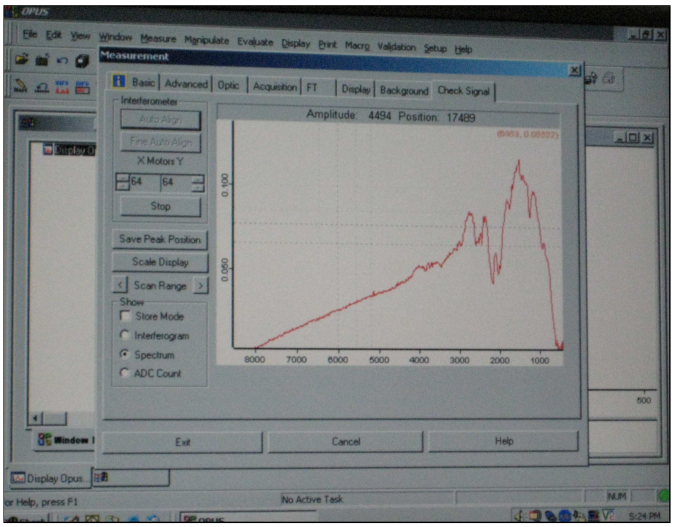

Figure 11: screenshot of software interface for transmittance

TATB and KBr powder are on one side of the sample chamber, and the other side has only KBr pressure transmitting media. This method allows for a non-sample background measurement at each pressure. Experiment #2 (far-IR) utilized petroleum jelly as the pressure transmitting medium,

and experiment #5 utilized no pressure transmitting media (sample loaded "neat").

This procedural difference was necessary due to the absorption of the pressure transmitting medium. The absorption profile of petroleum jelly does not change across the desired pressure range, and hence only one background spectra was collected at the start of the experiment (petroleum jelly with no sample). Likewise, in experiment #5, a spectrum of only the diamond culets placed together served as the background for the entire experiment. For the mid-IR experiments, a background pattern was required for every pressure because the IR spectra of KBr changes from ambient to 40 GPa (for example, there is a phase change at 2 GPa).

In all experiments, after the proper sample thickness was found, the DAC was then assembled completely with the screws kept loose in order to maintain an ambient pressure inside the sample chamber for the first measurement.

Ruby Pressure Sensor Measurement

The sample was placed in a Raman / ruby fluorescence system, with a 532 nm laser line and intensity no more than 20 mW at the sample. This system utilized a 1500 lines/mm grating, which was calibrated on the first day of each experiment with an He:Ne lamp. Care was taken to expose the sample in the laser light for brief periods of time, as TATB has shown evidence of damage under exposure to intense visible light[4]. A picture of the DAC and Jobin Yvon-Spex spectrometer (HR 460) used in the experiments is shown below in Fig. 12:

An ambient pressure ruby fluorescence spectrum was taken before pressurization of the sample for each experiment. The ruby R1 reference wavelength (694.39 nm) differed by less than 0.1 nm across the different samples. This reference wavelength was then utilized in the spectrometer software to provide the correct offset ($\lambda - \lambda_0$) for each successive measurement to calculate pressure (see eq/fig 19).

Pressurization

The symmetric DAC has four pressurizing screws, each with 29 beveled washers. The washers were arranged in following orientation: $<<<<><<<<>>>><<<<>>>><<<<>>>>$ (where $<$ and $>$ represent the beveled washer orientation). Two of the screws are counter-threaded, such that pressurization is accomplished by turning two opposing screws of the four holes simultaneously. After all screws were "finger-tight", they were tightened with two Allen wrenches in a alternating two-cycle procedure (two pairs of turns for four screws). No more than $^1/_4$ of a full turn was applied to each screw during a cycle. The lower pressures required several sets of turns

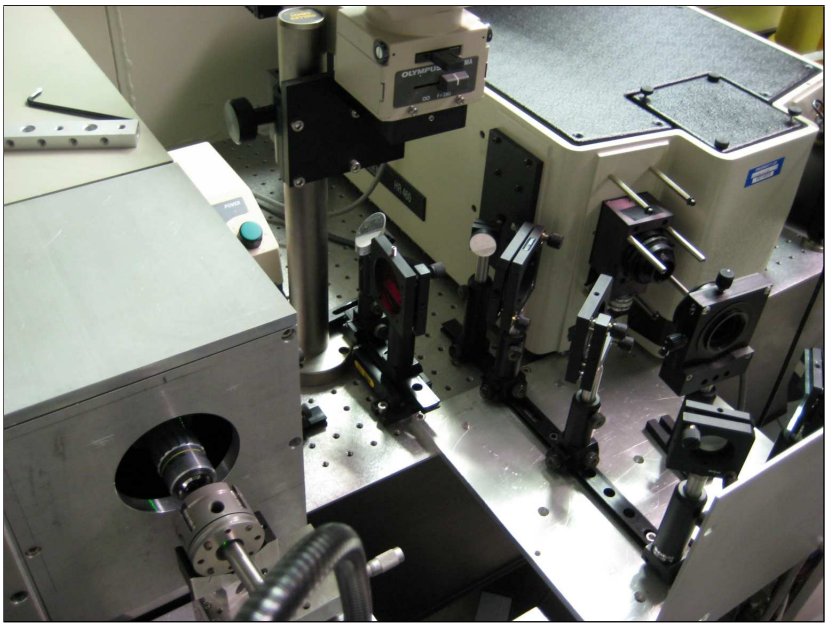

Figure 12: DAC on left, spectrometer on right, CCD on right off-picture

(up to two full turns to achieve a pressure of under 2 GPa), while at higher pressures (25 GPa), less than a $^1/_8$ turn resulted in a pressure change of 3 GPa. Fig. 13 depicts arrangement of the DAC and wrenches used during pressurization.

Stability of pressure in the sample chamber was verified by collecting ruby fluorescence spectra immediately after pressurization, and then several minutes later after IR data collection. While increasing pressure, there were negligible differences in the R1 peak wavelength between these measurements. This indicated negligible relaxation time during increases in pressure.

Before the conclusion of each experiment, the screws were loosened to decrease sample pressure and collect IR data for a reversibility check. During pressure decreases, there were noticeable pressure differences as indicated by the ruby fluorescence spectra. The greatest difference between pressure points was 3 GPa, after allowing the DAC to relax for several hours. When time permitted, a new IR spectrum of the sample was collected and the latter pressure determination utilized in data analysis. In other cases, the before- and after-IR data collection pressure measurements were averaged.

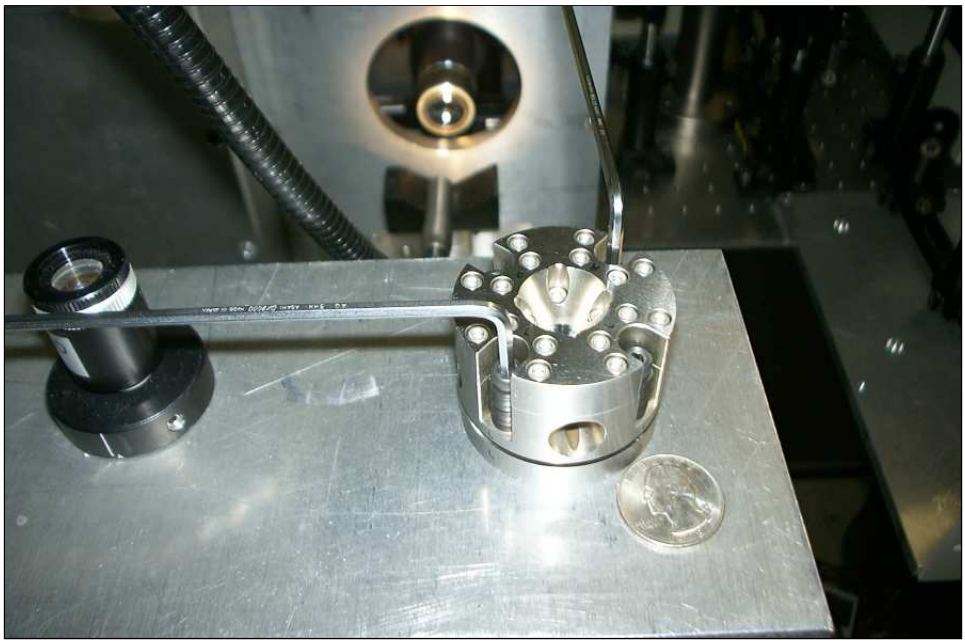

Figure 13: DAC pressurization. A quarter is displayed for relative size comparison

IR Spectra Collection

While far- and mid-IR data are collected with the same interferometer and computer setup, the collection optics and detectors differ. Consequently, the DAC is placed in different locations in the infrared beam path. Placement of the DAC is shown in the pictures below (Figs. 14, 15, 16):

Since both mid- and far-IR measurement locations are system-optimized to accommodate a symmetric DAC, very little fine-tuning was required between segregated measurements. The infrared beam aperture was opened to near the sample chamber diameter (120 microns), and positioning of the DAC within the beam did not need to be adjusted between measurements. For mid-IR measurements, the aperture of the beam was approximately 20 x 20 microns. It was necessary to adjust the location of the DAC within the beam for each pressure using an adjustable translation stage. A mirror is rotated into the infrared beam path, and visible light back-illuminated the sample area to determine proper positioning of the beam relative to the sample. In addition, the U2A synchrotron source inherently contains a portion of light in the low energy tail of the visible spectrum. This convenient ?feature? allowed for visual verification of the beam within the aperture. A picture of TATB, situated in the DAC for high pressure mid-IR data collection, is shown below in Figs. 17 and 18. Fig. 17 shows a sample of TATB at 15 GPa under a sample-loading microscope. A ruby

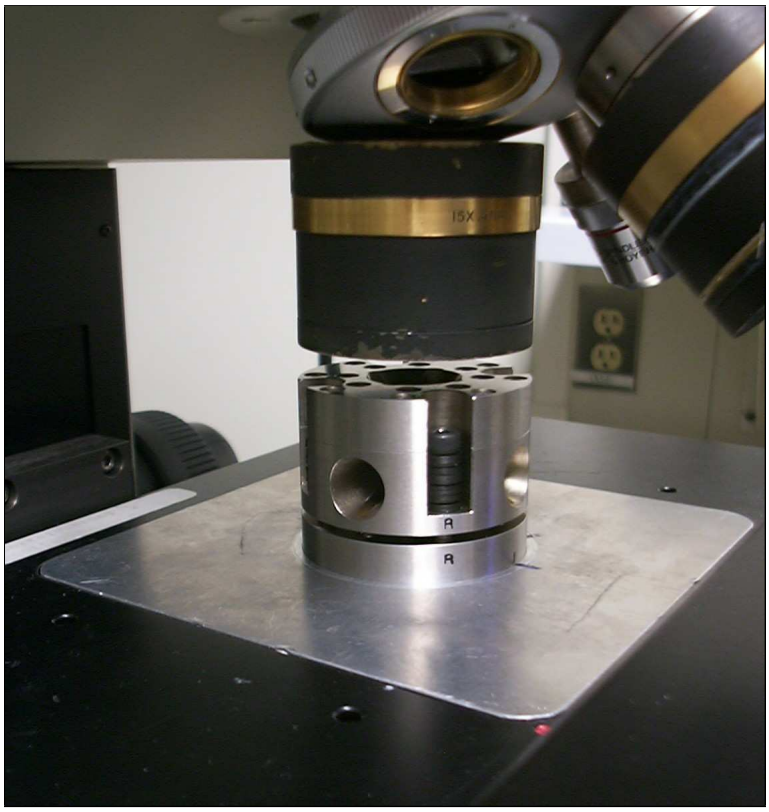

Figure 14: Zoomed-out view of DAC placement, Mid-IR

ball can be seen in the lower right (5 o'clock position) of the sample chamber. Fig. 18 shows the same sample in the Bruker mid-IR scope, illuminated from below by visible light with the aperture positioned over the area of the sample chamber containing only KBr medium.

Interferometer control was managed entirely by the OPUS® software. For mid-IR experiments, the software performed 1024 scans of the interferometer, with a resolution of 4 cm-1. Far-IR measurements were conducted similarly, with 512 scans instead. Upon completion of the desired number of scans, OPUS automatically combined all scans into one interferogram. This interferogram was normalized, background-subtracted, and Fourier-transformed immediately by OPUS®. The sequence of scans, followed by averaging, subtraction, and mathematical transform, constituted one measurement. Each OPUS® file, in native format, contains one measurement. For analysis in other software, both the absorbance spectrum and interferogram may be exported as two-column text.

The sampling time required for each measurement was about 7 minutes for mid-IR data col-

Figure 15: Zoomed-out view of DAC placement, Far-IR

lection, and 13 minutes for far-IR data collection. (Note: since mid-IR measurements required acquisition of a background spectrum for each pressure, the data collection time per pressure was actually 14 minutes.)

Minimizing Error / Miscellaneous Corrections

Consistency within the sample was verified at random times throughout the experiments by taking sample spectra within different regions of the sample chamber. There were no significant differences between the spectra; intensities of modes fluctuated minutely, and peak positions were unaffected. In addition, fluorescence spectra of ruby in different positions within the sample chamber were similar.

Spectra similarity indicated a quasi-hydrostatic pressure distribution at lower pressures. At higher pressures (above 25 GPa for experiment 4, and 20 GPa for experiment 5), broadening of the R1 fluorescence peak became more pronounced. However, as these experiments were completed between 30 and 40 GPa (to maintain integrity of the diamonds), the non-hydrostatic condition only affects the latter data points

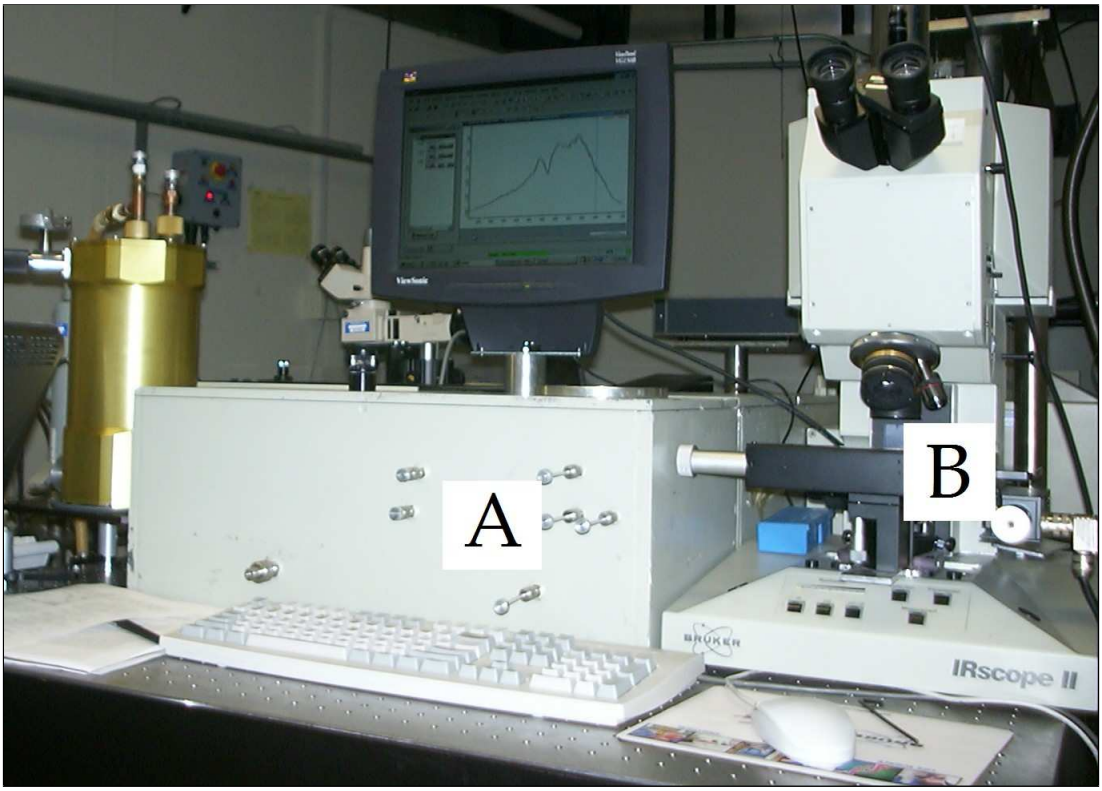

Figure 16: "A" marks location for Far-IR measurement; "B" marks Mid-IR location

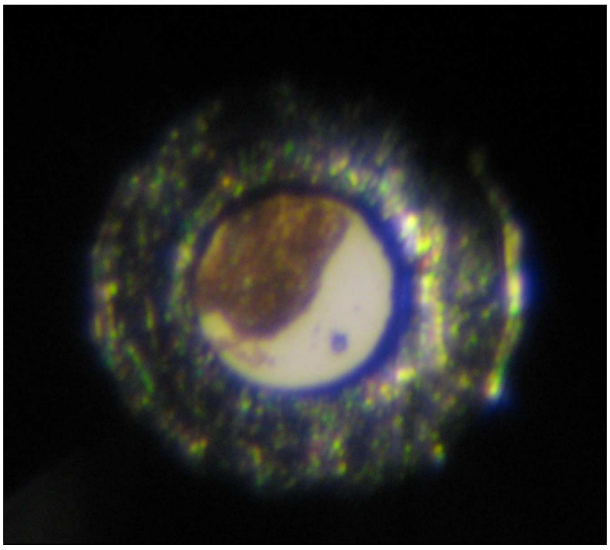

Figure 17: Sample at 15 GPa under a sample-loading microscope

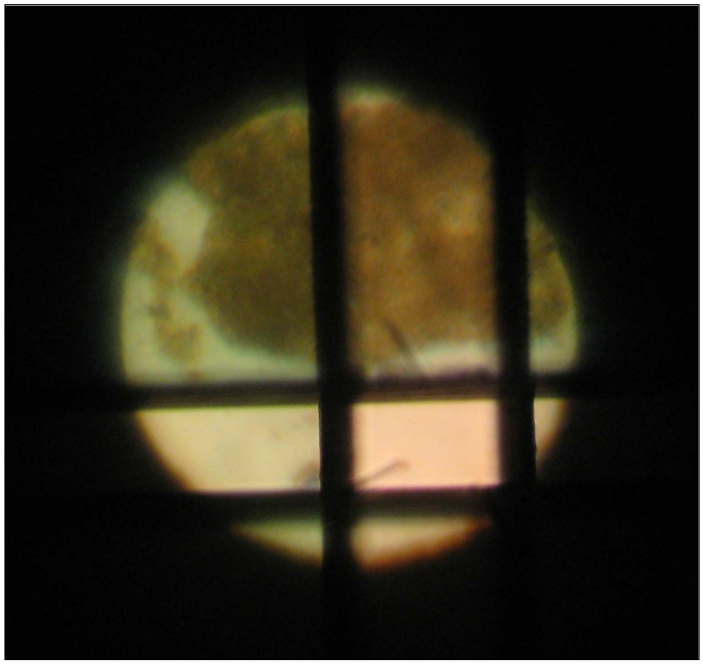

Figure 18: Sample at 15 GPa under mid-IR scope

CHAPTER 3

DATA ANALYSIS

Pressure Determination & Validation

Thermally annealed ruby spheres were the only pressure sensor utilized in the experiments. Experiments 4 and 5 also included more than one ruby ball in the sample chamber, so pressure gradients could be checked. For all collected ruby spectra, the Mao-Xu-Bell scale (1986; see Eq. 3.1 below) was used to determine pressure in the sample chamber of the ruby. Since the pressure ranges used in all experiments were relatively low, and the temperature held at 298K, it was not necessary to use any of the more recent Ruby calibrations (Syassen).

$$P = \frac{A}{B}\left(\left[1 + \left(\frac{\Delta\lambda}{\lambda_0}\right)\right]^B - 1\right) \tag{3.1}$$

(in Eq. 3.1, P is pressure in GPa, A = 1904 GPa, B = 7.665 [H. K. Mao, J. Xu, and P. M. Bell, J. Geophys. Res. 91, 4673 (1986).])

The position of the R1 fluorescence peak was determined by two methods: visual inspection and Lorentzian curve fitting. The visual method was a faster and direct approach, most useful while actively collecting spectra. The R1 and R2 peaks were displayed in their entirety on the fluorimeter's computer screen and a cursor could be used to navigate across the spectrum to read position and intensity coordinates. The installed WinSpec® software automated the wavelength-to-pressure conversion via the above Mao-Xu scale. Hence, when the cursor was visually placed at the full-width, half-maximum (FWHM) position, pressure could be immediately read from the screen.

Though the visual technique expedited the data collection procedure while at the beamline, all fluorescence spectra for experiments 3, 4, and 5 were recorded for future analysis by curve-fitting. In addition to verifying the precision of the visual inspection method, it is useful to have a record of the R1 fluorescence wavelengths associated with each IR spectrum collected. Since the ruby scale is a function of fluorescence wavelength (at fixed temperature), future refinements to the ruby calibration scale could be easily incorporated in these data and results.

The multi-peak fitting routine of the Origin® software package was used to re-determine the R1 peak positions of collected spectra. Shown below (Fig. 19) is a sample of the fitting procedure for a ruby fluorescence spectrum of TATB near ambient pressure:

In this example, the R1 peak position is determined to be 694.42 nm, with the uncertainty in

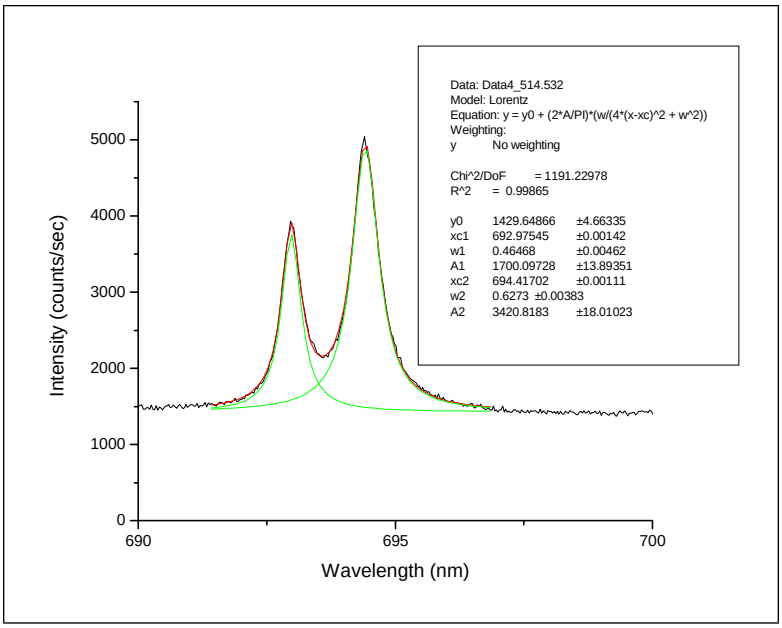

Figure 19: Ruby fluorescence spectrum at low pressure

the fit lower than the uncertainty of the measurement (0.1 nm). In addition, the curve fitting method for lower pressures was shown to be negligibly different from the results of the visual inspection method. Above 20 to 25 GPa, differences in the visual and fitting methods become more pronounced. This was caused by the increased broadness of the R1 fluorescence peak. Shown in Fig. 20 is an example of a best fit to a fluorescence spectrum of poor quality.

The increased broadness of the R1 fluorescence curve indicates the ruby sphere is no longer in a hydrostatic condition in the sample chamber. This may be due to the existence of deviatoric stress, pressure gradients, or a combination of both. In the case of experiment 3, it is likely the ruby came into contact with the top and bottom diamond culet, bridging the culets. In this situation the pressure sensor is completely unreliable, so the DAC needs to be reloaded.

After all the ruby R1 pressure measurements for the experiments were analyzed, it was made aware that analysis could also be done with the R2 line shift (cite: Y.M. Gupta, X.A. Shen. Potential use of the ruby R2 line shift for static high-pressure calibration). Shock compression experiments show the R2 line shift is independent of crystal orientation.

Data Transformation to IR Vibrational Spectra

Since the interferometer is placed behind the DAC in the IR beam, the raw data (an interferogram) is a measurement of transmitted light intensity. The proprietary OPUS® software automati-

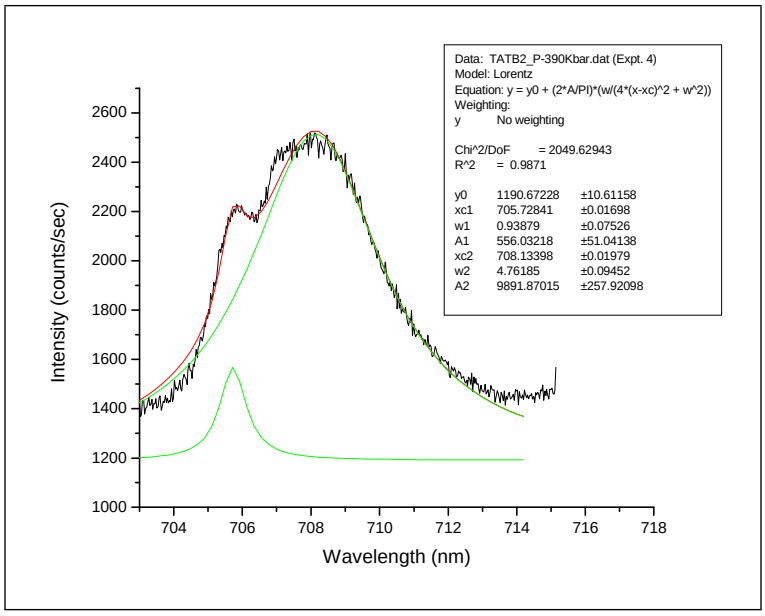

Figure 20: Ruby fluorescence spectrum at high pressure

cally performs a fast Fourier transform on the intensity vs. mirror position interferogram to obtain an intensity versus wavenumber spectrum. The free parameters in the transform (e.g. normalization factor) are calibrated by the beamline scientist prior to the allotted beamtime, and are fixed for all IR (one set for far-IR; one set for mid-IR) transmission experiments. As a result, the output of the Fourier transform is computed to 10 significant figures and intensity values ranging from -6 to +6. The precision of this computation is several orders of magnitude higher than the instrumental precision, and is therefore a negligible factor in the error analysis.

OPUS®) then converts the transmission spectrum into a background-subtracted absorbance spectrum using the following formula:

$$I_{sample,absorbance} = -\log \frac{I_{raw,transmission}}{I_{0,background}} \tag{3.2}$$

The OPUS® software's absorbance calculations consider the absorption as the inverse of the transmitted light. The theoretical calculation of absorbance, in addition to transmission data, requires reflection measurements. While transmittance and reflectance data can be utilized to determine the complex index of refraction of the sample[11] as a function of frequency, the purpose of these experiments primarily entailed identification of vibrational modes. Since the sample thickness is optically thin (on the order of microns), the index of refraction is assumed near 1. This

approximation is valid for mid- to far-infrared radiation if

$$\frac{n\omega d}{c} << 1 \tag{3.3}$$

where n is the index of refraction, d is the sample thickness, ω is the frequency, and c is the speed of light[11, 12]. As a result, the reflectance is assumed to be negligible compared to the absorbance, and the sample absorbance is a function only of transmitted light.

Since water absorption and slight fluctuations in the synchrotron beam intensity can distort individual spectral intensities, each spectrum is renormalized in Origin® and plotted together (vertically stacked spectra) to exhibit qualitative changes in vibrational modes. Spectra from experiments 3, 4, and 5 are shown in Figs. 21,22,23 (the spectra from experiments 1 and 2 have been published; see vita).

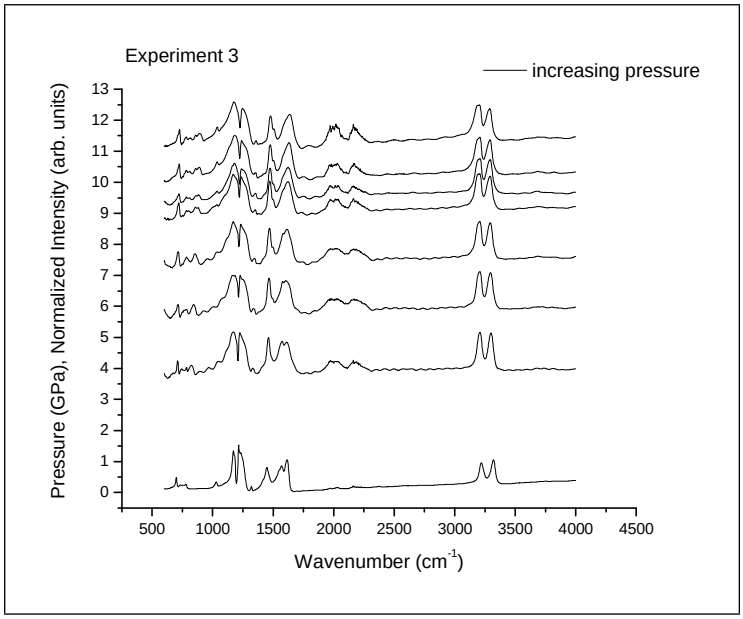

Figure 21: Experiment 3 spectra

Determination of Vibrational Mode Trends

A selection of modes for analysis was chosen primarily based upon ease of their visual identification and distinct separation within the spectra. For instance, while the vibrational modes around 1200 cm^{-1} (see Fig. 22) are prominent, there are likely more than two overlapping modes in that

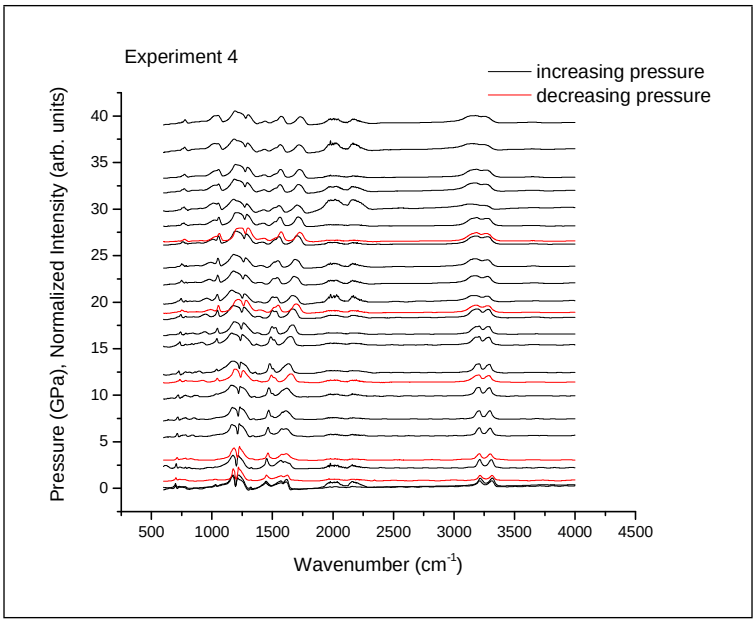

Figure 22: Experiment 4 spectra

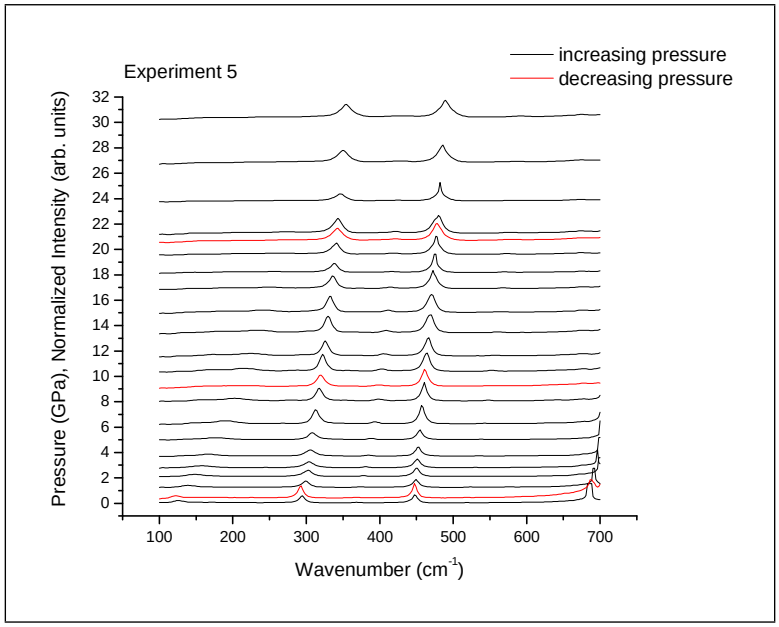

Figure 23: Experiment 5 spectra

narrow frequency range. Multi-peak fitting becomes increasingly difficult at this level of analysis, as the number of fit parameters increases beyond the ability of physical knowledge or intuition to

make logical guesses for highly coupled parameters. An example will be shown that demonstrates the ambiguity in number of peaks fit to the experimental data.

Some modes, both relatively weak and strong, could be easily distinguished from neighboring modes due to narrow peak widths. These modes were fit with single Lorentzian curves. Similar to the fit procedure for the ruby fluorescence spectra, the choice of Lorentzian curve fitting (instead of Gaussian or Gaussian-Lorentzian convolutions) was based on better-refined and fewer fit parameters. While there were likely thermal and instrumental variances in modes, contributing to a Gaussian profile, the Lorentzian profile appeared to be the dominant contribution. Additionally, the fit procedure returned parameters with higher precision than the actual measurement resolution (in both frequency resolution and pressure). An example of the fit procedure for single peak analysis is shown in Fig. 24.

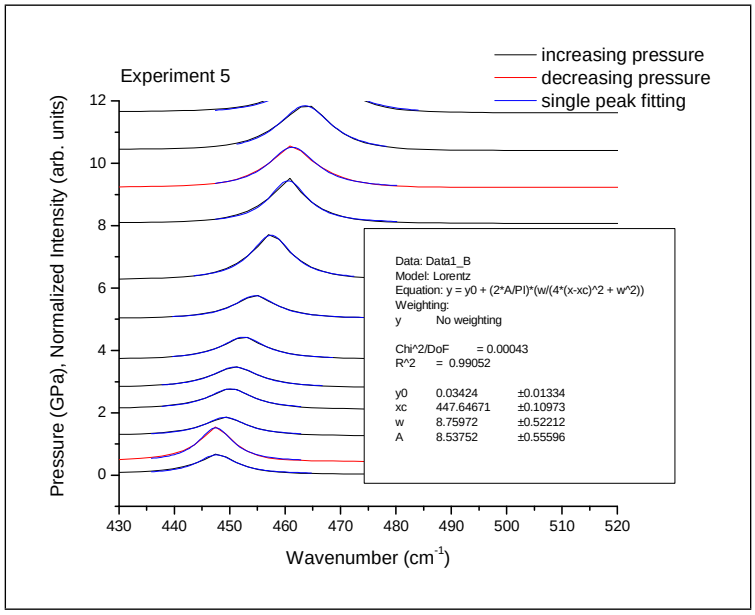

Figure 24: Lorentzian fit example, one-peak routine

As pressure was increased, many modes broadened. Consequently, while some modes could be easily distinguished at lower pressures, they exhibited strong overlapping at higher pressures. For consistency, these modes were analyzed through the entire pressure range with multi-peak fitting. A good example of this procedure is shown in Fig. 25

It is noted that while the two-peak fit procedure for the above spectra produces visually accurate models of the modes at lower pressures, the fit error increases significantly at higher pressures. The

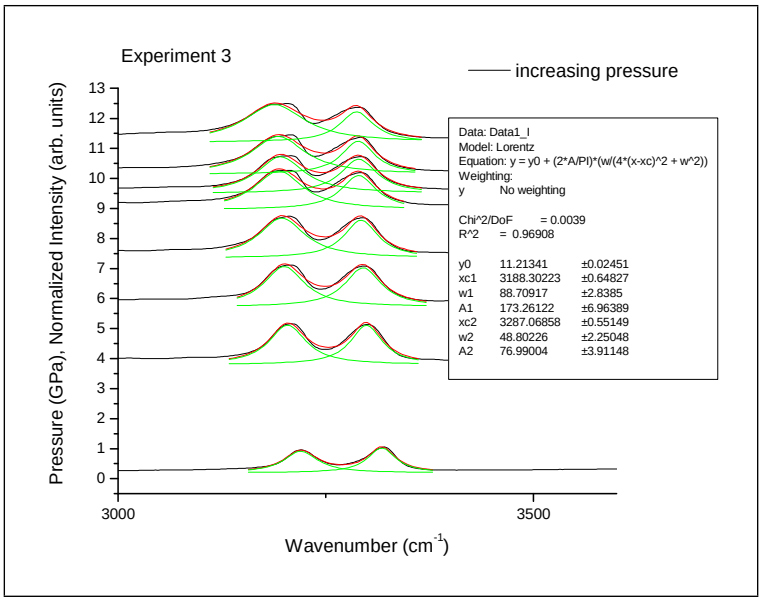

Figure 25: Lorentzian fit example, two-peak routine

physical inferences will be discussed in the next section; the immediate consequence to the model is that the number of free parameters must be increased. Several attempts were made to fit high pressure vibrational modes to 3 or 4 peaks, when only two modes could be easily distinguished. The two graphs in Figs. 26 and 27 show 4-peak fits to the same frequency range.

While the results of these fits show a closer correlation of peak-fitting model to data (the reduced χ^2 value decreases), a plot of peak position vs. pressure indicates a less likely physical trend. In other words, because the fit parameters have been increased, the fit appears better; however, there is no sufficiently likely physical explanation for increasing the number of fit parameters (see Fig. 28).

Instrumental and Fitting Error Considerations

Fig. 29 incorporates error bars to show the relative weight of a given peak fit position. The error in the pressure is taken to be 5% relative to the measured value, and the error in the peak position is a fixed value of 5 cm^{-1}. During the pressure measurement, there was a general deviation in the ruby fluorescence measurement, which averaged to be approximately 0.1 nm for the lower pressure points. For higher pressure spectra, a non-hydrostatic condition causes the fit of ruby fluorescence spectra and average pressure in the sample to be greater. As all experiments conducted had only one ruby sphere in the sample chamber, it was not possible to measure a pressure gradient across

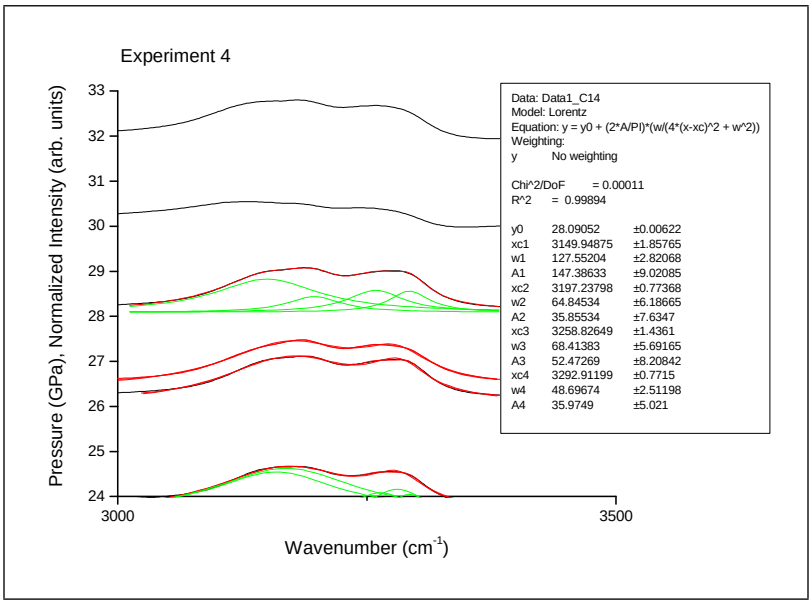

Figure 26: Lorentzian fit example, multi-peak routine at high pressure

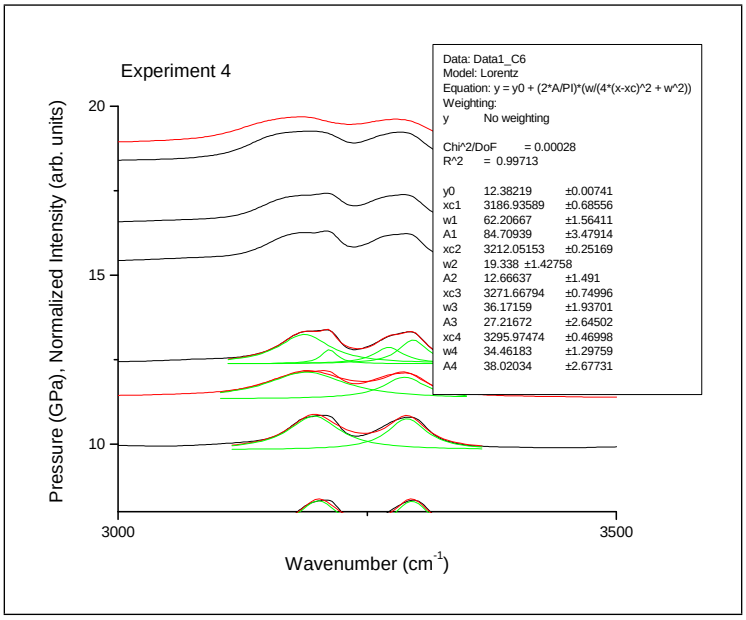

Figure 27: Lorentzian fit example, multi-peak routine at moderate pressure

the sample chamber. Consequently, as the pressure increased beyond the quasi-hydrostatic condition, the relative error of 5% in pressure is likely underestimated. This can be connected to the error in the fit routine, as the ability to fit a Lorentzian profile to the data became more difficult. The

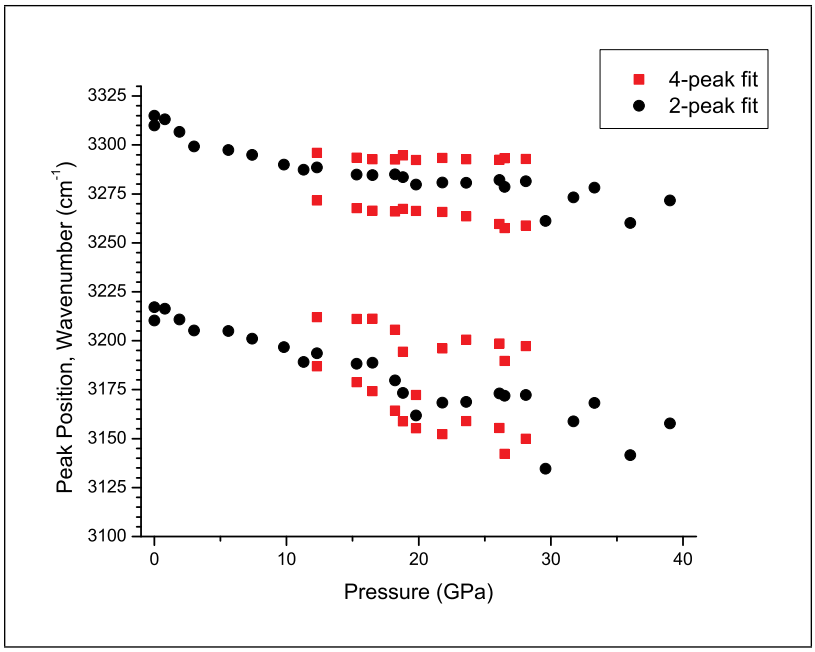

Figure 28: 4-peak and 2-peak fit routines overlayed

instrumental resolution was 4 cm^{-1}, but the spread in the peak positions ranging between 3 and 10 cm^{-1} (see Figs. 30 and 31) suggests an error around 5 cm^{-1} for better quasi-hydrostatic conditions. In particular, the poor quasi-hydrostatic conditions above 30 GPa in experiment 4 suggest an increase in the error bars. Without a more rigorous method of analysis (with multiple ruby spheres to determine pressure gradients), it is not possible to quantitatively assign increased error bars for this higher pressure range.

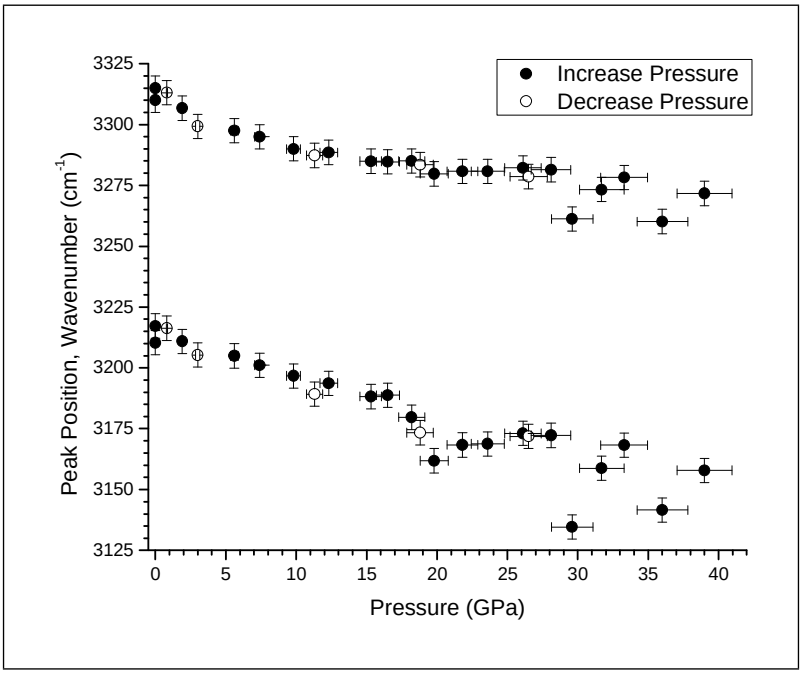

Figure 29: Mode frequencies vs. Pressure, 3200 $cm^{-}1$

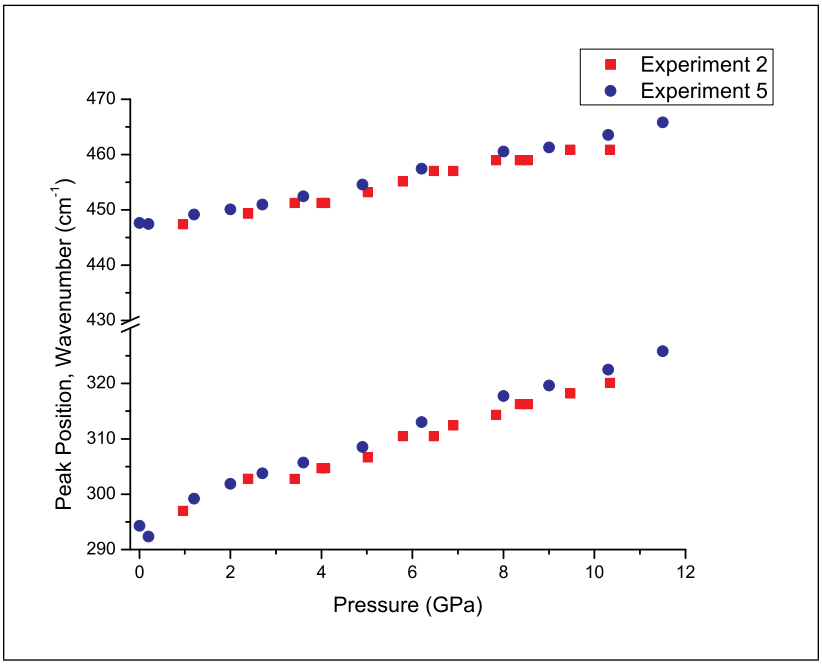

Figure 30: Comparison of frequencies across experiments, Far-IR

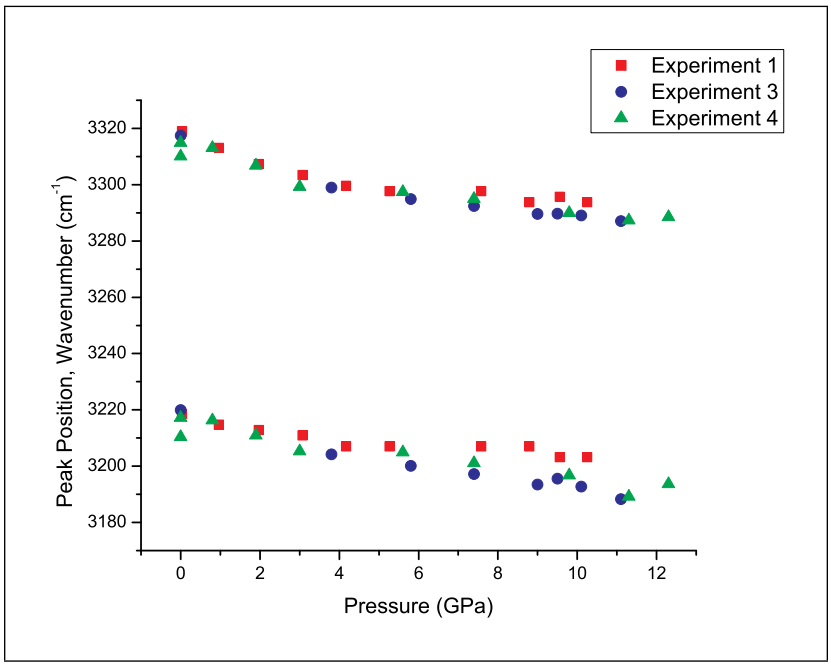

Figure 31: Comparison of frequencies across experiments, Mid-IR

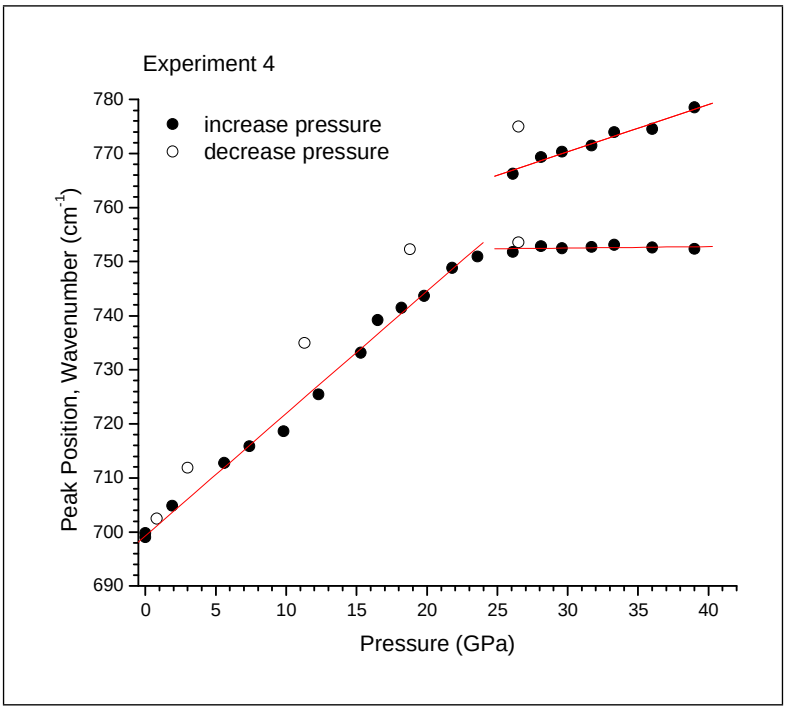

Figure 32: Mode frequencies vs. Pressure, 700 cm^{-1}

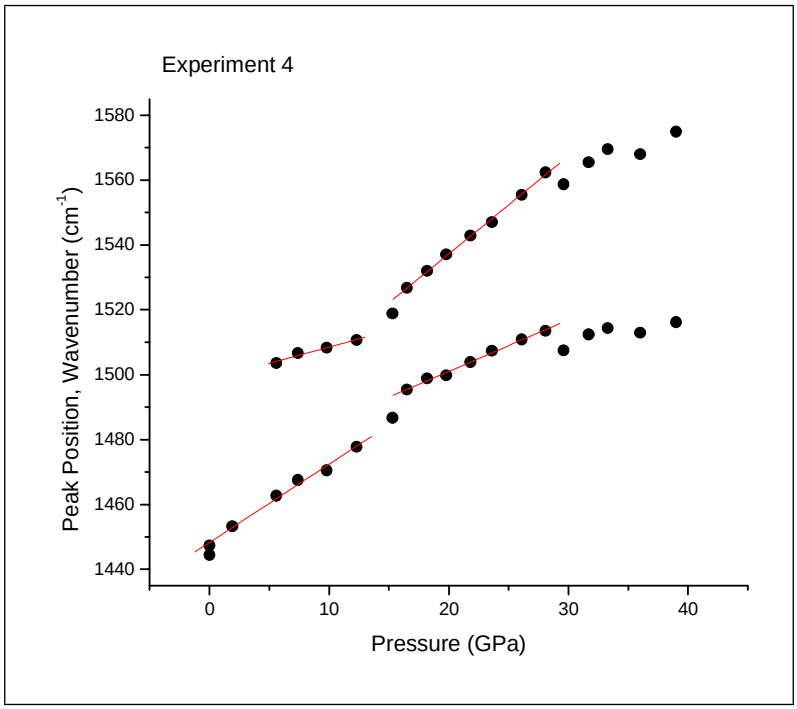

Figure 33: Mode frequencies vs. Pressure, 1440 cm^{-1}

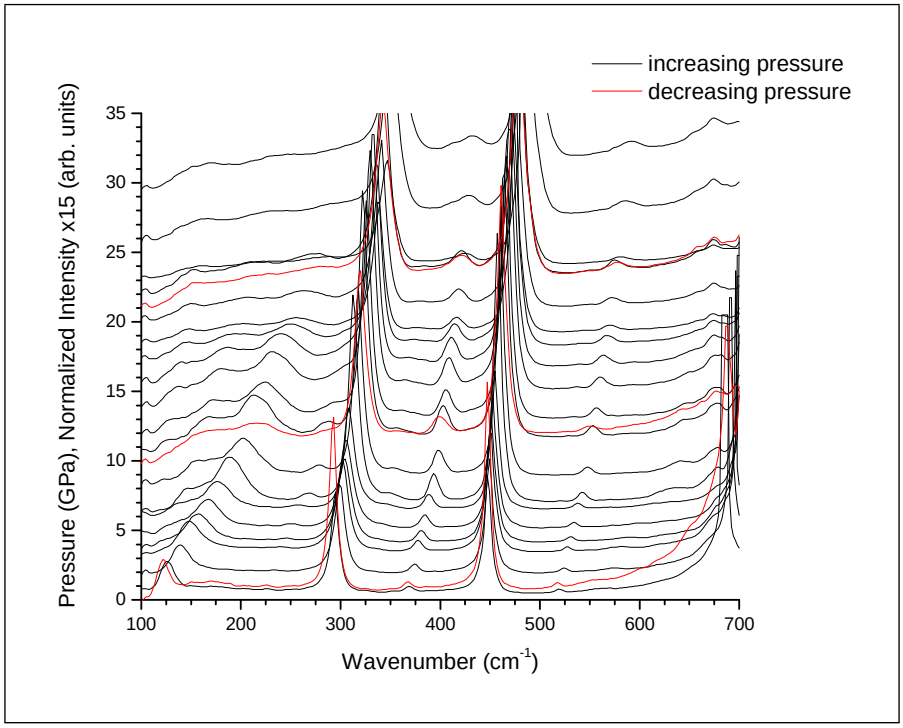

Figure 34: Experiment 5 spectra, enhanced intensity

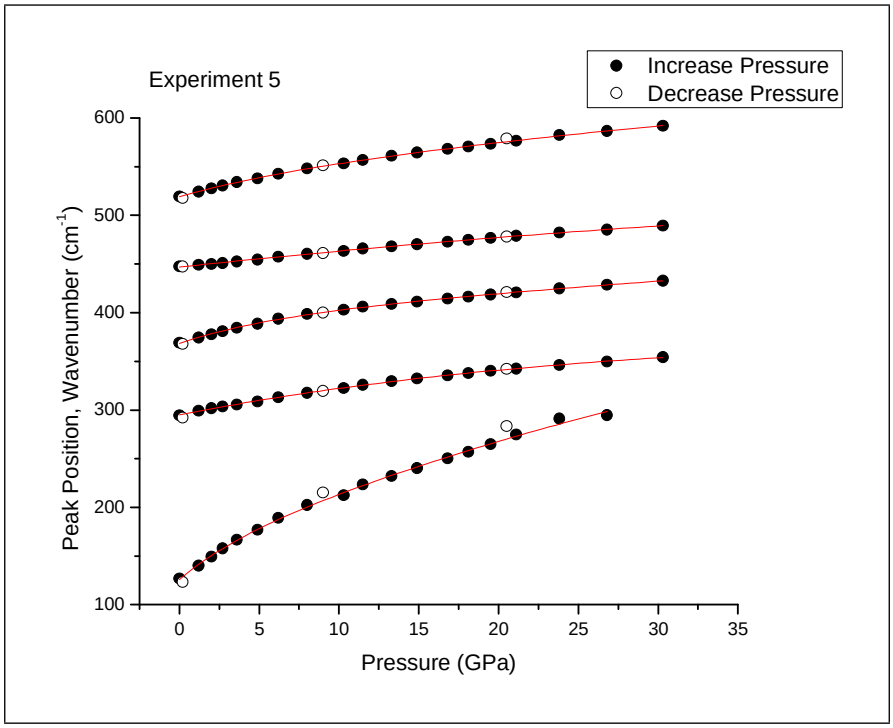

Figure 35: Mode frequencies vs. Pressure, Far-IR region

CHAPTER 4
RESULTS & DISCUSSION

Primary Observations

The main goal of this project was to witness any possible phase changes in TATB under high pressure conditions. By inspection of the spectra in the far- and mid-IR region (Figs. 22 and 23), the initial observation is that no high-intensity modes appear or disappear in the studied pressure range. As the observed vibrational modes are indicative of the molecular and crystallographic symmetry, the appearance or disappearance of prominent modes is the first suggestion of a change in symmetry[13]. Regardless of any anomalous trends seen through a more detailed analysis, the primary conclusion is that TATB undergoes no significant molecular or crystallographic change in symmetry under the ambient to 35 GPa pressure range. Based on this work and recent studies (Dattelbaum), there is no strong evidence to suggest TATB undergoes any phase changes between ambient and 35 GPa.

Normal Trends of Normal Modes

Most observed vibrational modes increase in frequency as pressure is applied. This is the expected behavior, as the modal frequency scales with the force constant (in the harmonic approximation). The force constant is a quantification of the stiffness of the "spring" between atoms in the molecule (relating to chemical bonding), and molecules in the crystalline lattice (intermolecular forces). From fundamental thermodynamic principles, an increase in pressure must be accompanied by a decrease in volume (when there is no structural phase change or chemical reaction). When the volume decreases, interatomic distances shrink, and stable (full) electron shells around individual atoms cause an increase in repulsive forces between atoms. This is analogous to the stiffening of a mass attached to a spring. The internal energy increases and the vibrational motion of the atom (or motion of a group of atoms in more complex normal modes) experiences an increase in frequency (in general).

The simple harmonic model of normal vibrational modes suggests that as the internal energy of the system is increased, the frequency of the normal mode (which is a function of the force constant of the interacting atoms and the atomic mass) should not change. However, an increase in pressure of necessity causes an increase in density, and so the atoms in a crystalline lattice are not located at the same absolute positions. Consequently, the inter- and intra-atomic potentials have different

equilibrium positions, and the shape of the potential well must change.

When a vibrational mode experiences a fixed change in frequency with respect to an incremental change in pressure, this linear slope is a measure of the first-order anharmonic behavior of the system. This value is labeled as the Grüeneisen parameter for the given mode[14].

Fermi Resonance

Fermi resonance is a consequence of the failure of the harmonic potential model to accurately describe the behavior of vibrational modes of the same symmetry species[9]. The simple harmonic potential model poses a Schrödinger equation with N atoms, linked by $(3N-5)$ or $(3N-6)$ "springs" between atoms (the number of springs depends on the symmetry of the system). A critical aspect of this model states that in order to solve the Schrödinger equation into eigenstates of the harmonic oscillators, they must be decoupled into normal modes.

In theory, a vibrational mode of one symmetry species (in this case vibrational modes corresponding to a particular orientation of the molecular dipole moment with respect to incoming infrared radiation) should be independent from another vibrational mode of the same species. Hence, while a change in the system's pressure will most likely affect all vibrational modes, the existence of any particular vibrational mode should not affect the frequency of excitation of another mode.

When modes of the same symmetry species approach a similar frequency, physical effects not described by the harmonic potential (i.e. anharmonic contributions) cause deviations in the predicted behavior of the vibrational states. Measured mode intensities can be enhanced, and something akin to a repulsion between modes of similar excitation energy can cause the prevention of overlapping or merging of frequencies of two modes. Also, as two modes experience corresponding frequency shifts with respect to pressure, the resonance effect can cause a swap of excitation energy between the two modes as they near each other in energy (the coupling causes an intensity enhancement). Hence, in the case of two modes increasing frequency at different rates as pressure is increased, at the point of theoretical crossing of those two rates (where both modes would share the same frequency) the rate change of one mode would become the rate change of the other, and vice versa. See Fig. 34; two modes that begin to merge, at 1500cm-1 and 18 GPa, exhibit this behavior and consequently the effect may be explained by Fermi resonance (provided a definitive normal mode assignment verifies the symmetry class)[9].

Decrease of Frequency with Increase in Pressure

While most observed vibrational modes display the expected increase of frequency with increased applied pressure, there are a few notable exceptions. Previous experiments[4] speculated on, and observed, a decrease in the frequencies of the amino (NH_2) and nitro (NO_2) groups under increasing pressure conditions. Unfortunately, the vibrational modes associated with the nitro groups could not be easily resolved with the current methods of analysis; however, the amino group symmetric and antisymmetric stretching modes are relatively isolated and verified this trend.

Figure (expt. 4, NH2 plot) shows a negative-sloping trend for both the symmetric and antisymmetric NH_2 stretches as pressure is applied. The best explanation for this first-order negative slope behavior offered pertains to hydrogen bonding of the hydrogen atoms in the amino group with the oxygen atoms of neighboring nitro groups (in the nearest-neighbor molecule).

As suggested by the prior studies, as the cell parameters adjust to allow for a decrease in volume as pressure is applied, the amino groups of one molecule are forced closer to adjacent molecules (both in the plane and in nearby layers). The orientation of one molecule to another suggests that the amino groups are met by nitro groups as nearest-neighbor atoms in the nearby molecules. Hydrogen's low mass and strong desire for a full s-shell allow it to move more readily than the other atoms in the molecule. The individual oxygen atoms in the nitro groups do not have full p-orbitals, due to the sharing of an electron across both oxygen atoms in the nitro group. Consequently, the oxygen atoms in the nitro groups become polarized and are also attracted to the nearby hydrogen atoms.

Since the effective mass in the nitro groups is much higher than the amino groups, the hydrogen atoms move away from the parent molecule more than the oxygen atoms from their parent molecule. As a result, the equilibrium position and shape of the potential well for the hydrogen-nitrogen vibrations is more strongly affected. The base of the well moves outwards and the shape of the well becomes shallower, causing a reduction in the effective spring constant. Since TATB is more compressible at lower pressures, the reduction of the spring constant (and hence the frequency of the vibration) is more drastic than at higher pressures.

The non-smooth behavior of these two modes, beginning around 17 GPa, may be interpreted by other minor effects contributing to the mode frequency in addition to hydrogen bonding. For instance, at approximately 17 GPa there is a sudden drop in the symmetric NH_2 mode (and to a a lesser extent the antisymmetric mode). Notice that the mode frequency in that region is approx-

imately 3170 and 3280 cm^{-1} respectively, and compare it to the full spectra from experiment 4, particularly modes in the 1500 and 1650 cm^{-1} region. These modes are roughly half the frequency of the NH_2 stretching modes, and overtones from the lower frequency modes may be coupling with the NH2 modes.

Overtones occur when incident light interacts with a harmonic oscillator to cause transitions to a higher vibrational state. While a fundamental normal mode is the result of a transition from the lowest vibrational state to the first excited state, it is possible to witness a transition from the lowest vibrational state ($n = 0$) to the second vibrational state ($n = 2$). This is known as the first overtone for the given mode, and is generally at a slightly lower energy than twice the fundamental mode (the potential well is not a true harmonic oscillator, so higher energy states are not exact multiples of the fundamental, and the selection rule of $n \rightarrow n + 1$ does not necessarily apply). As the modes in the 1500 to 1700 cm^{-1} range are of E′ symmetry along with the NH_2 modes[15], there is the possibility of interaction with the NH_2 modes.

Overtone contributions are a possible explanation for the abrupt shifts of the NH_2 stretching modes near 20 GPa and above, since as the NH_2 modes decrease in frequency, the assortment of modes in the 1500 cm^{-1} region increase in frequency. As a result, overtones from several lower frequency modes may be affecting the NH_2 stretching modes.

Reversibility and Possible Dimerization

After compressing the sample to above 30 GPa, experiments 4 and 5 test for reversibility by decompressing the sample to ambient pressure conditions. Several pressure and infrared measurements were taken along this path to ambient pressure, and the DAC was allowed to stabilize for a period of several minutes to a few hours between decompression measurements. This minimized the effect of any time-dependent relaxation processes, and any deviation in the peak positions at the same pressure (as shown by the labeled points in Fig. 32,33) which is an indication of hysteresis.

Most analyzed modes returned to their original frequencies upon decompression to ambient pressure, and visual inspection with an optical microscope showed the color of the sample to be identical to that of the virgin uncompressed material. This indicates that regardless of any possible higher-order phase changes, TATB demonstrates no major structural or chemical changes under compression in a DAC to 35 GPa.

It is possible that there are still minor structural changes occurring under these extreme conditions because a few analyzed modes in the far-infrared region showed a deviation from ambient pressure conditions upon decompression (see Fig. 35). If a particular normal mode increases in fre-

quency as pressure is applied, and returns to a frequency slightly higher than the original frequency when the applied pressure is released to ambient, it is most likely explained as a relaxation of the DAC or hysteresis effect of the sample. Modes displayed in Fig. 35 displayed anomalous behavior because the mode frequency after release is slightly lower than the original frequency. Errors in peak fitting may explain the discrepancies as the effect appears at the boundary of the error bars. But if the effect is not due to technical or instrumental deviations, it could be an indication of a fine structural change. Because these modes are associated with weaker force constants and increased masses (lattice modes describe the intermolecular interactions), they tend to be more sensitive to changes in the overall crystallographic structure.

The TATB molecule is planar and arranges itself in a lattice in layers. While it may be logically (yet crudely) anticipated that the high molecular symmetry lends to a hexagonal crystallographic structure, previous experiments have verified the triclinic nature of the system. This is primarily due to the stacking of molecules along the c-axis (out of the plane of the molecule). The cell angles are similar to the parameters for a monoclinic cell, and hence macroscopic TATB single crystals have a hexagonal-looking appearance (see Fig. 36). On the microscopic level, small shifts in the arrangement of the molecular sheets relative to each other could result in a new structure of equally low symmetry. The overall cell volume may retain a similar size while the bond angles would adjust to allow the distortion. In addition, group symmetry rules predicting the absence of some vibrational modes may not change.

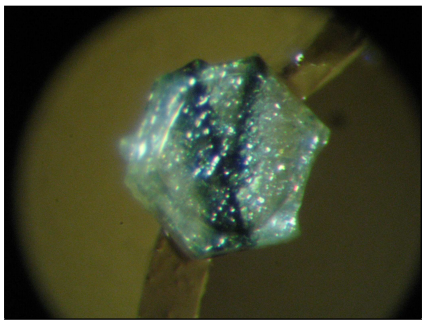

Figure 36: TATB single crystal, with radiation damage tracks

Consequently, the behavior of TATB under compression may vary with different pressure regimes. While the poor quasihydrostatic conditions above 20 GPa may cause these anomalous vibrational mode trends, the behavior may also be explained by changing relative shifts in cell angles. While

the overall structure is still triclinic, the system may experience varying distortions under increasing pressure conditions.

Additionally, high pressure conditions force greater inter-molecular interactions. It has been suggested (Dattlebaum) that TATB dimerizes under high pressure conditions (above 9 GPa). While this experiment can neither prove nor disprove dimerization theories, the lowered mode frequencies after release to ambient conditions may offer indirect evidence to an irreversible dimerization. If TATB molecules across layers are forced to interact, and achieve a mild level of coupling, this condition may persist after decompression. Any attraction between molecules will result in a weakening of the associated lattice vibrational modes. The lowest analyzed modes in Experiment 5 (most notably 125 and 290 cm^{-1}) indicate lowered frequencies after the sample was released to ambient pressure. While it is not enough evidence to prove dimerization in TATB with pressure, the possibility exists and can by weakly supported by this data.

Correlation with Kinetics Experiment

An interesting observation entails a possible correlation between vibrational mode anomalies from these experiments and experimental data on reaction propagation rates (RPR) in TATB[16]. The previous experiment measured the reaction propagation rate in TATB in a diamond anvil cell held at different pressures (note reproduction of plot from original paper in 37). The reaction propagation rate shows several discontinuities in an otherwise somewhat linear trend of RPR vs. pressure. Most notably, around 19 GPa and 30 GPa, the RPR drops substantially (also, if the Fultz experiment had been conducted to higher pressures, there may be another discontinuity around 38 to 41 GPa). Comparing these points to the vibrational modes starting at 1440, 1500, and 3220 cm^{-1} (Figs. 33 and 29), there appear to be similar deviations from otherwise linear trends in the same pressure regions.

This correlation may be mere coincidence, or it may signify a relationship between vibrational mode trends and the RPR with pressure. As current models on detonation theory are still very uncertain of the exact mechanism causing deflagration and detonation at the molecular level, it is reasonable to suppose that there may be a physical relationship between these two seemingly independent measurements. Qualitatively, one assumes[6] that the nitro and amino groups in HE molecules are likely to play a critical role in the mechanism of initiation. Consequently, pressure-dependent behavior of the normal modes associated with the nitro groups may have an effect on the overall initiation process.

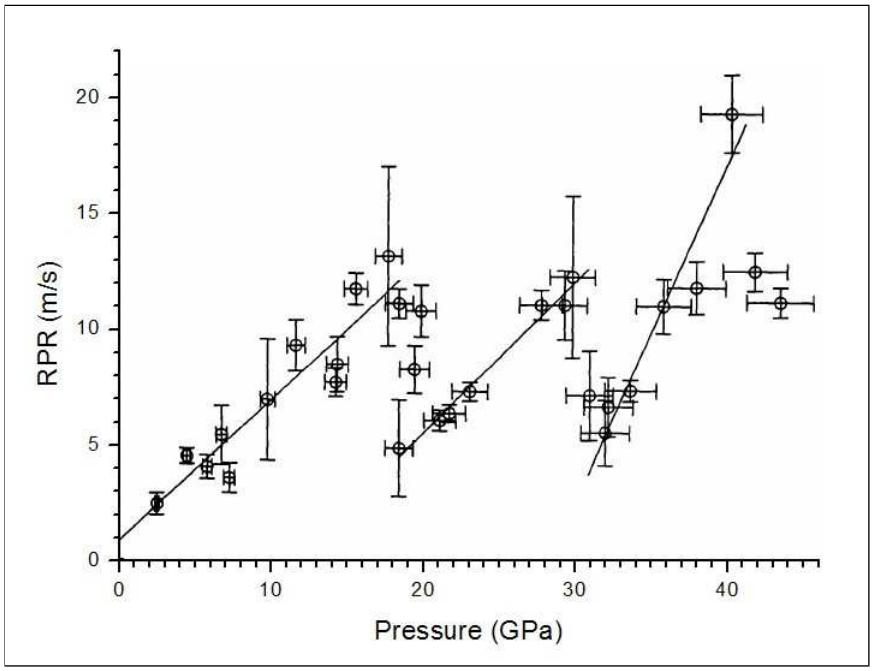

Figure 37: Regeneration of RPR plot from data from Foltz

CHAPTER 5
CONCLUSIONS

The behavior of the TATB molecule in the solid state and crystalline structure under high pressure conditions is not a simple molecular system. Though the evidence presented in this project does not support the existence of a high pressure crystallographic phase of TATB, the behavior of the vibrational modes under varying pressure warrants further investigation beyond the scope of these experiments. Non-linear and disjointed trends observed with increasing pressure indicate anharmonic behavior of many normal modes. Though hydrogen bonding, vibrational overtones, and mode coupling (in the form of Fermi resonance) are viable explanations for some of this behavior, the present set of infrared spectroscopy experiments cannot support these interpretations beyond all reasonable doubt.

As TATB is of great interest for military and industrial applications, and has been shown to be more insensitive than other conventional high explosives, this study presents data useful for understanding the behavior of TATB under extreme conditions. These data continue support of previous conclusions[4] that TATB has no high pressure phase, which is a unique property among other materials of the same category (iHEs).

In addition, the decreasing frequencies of the modes associated with the amino group lend further support to the idea that hydrogen bonding plays an important role in the stability of energetic materials.

A notable observation is that the Chapman-Jouget (CJ) point of TATB is at a lower pressure than the pressure range of these experiments (which showed a recoverable sample). This implies that dynamic shockwave experiments have fundamentally different effect on this (and likely other) energetic materials. Further study should aim to characterize these differences. While static diamond anvil cell work is useful for extracting the physical properties of these molecular systems with pressure, these materials are ultimately used in a dynamic environment.

Future studies should investigate the anomalies in the TATB vibrational modes between 20 and 30 GPa (and beyond), by attempting to achieve a better quasi-hydrostatic condition with different pressure-transmitting media, and by sampling other techniques (such as single crystal Laue diffraction) and with finer pressure increments. Further detailed studies can provide a better link to the dynamic behavior of TATB as well as leading to an overall more fundamental understanding of highly energetic materials and their reliability and usefulness in modern technological times.

REFERENCES

[1] C. Jackson and J. Wing, Am. Chem. J. **10** (1888).

[2] B. M. Dobratz, Los Alamos National Laboratory LA-13014-H **131** (1995).

[3] H. Cady and A. Larson, Acta Crystallogr. **18** (1965).

[4] S. Satija, B. Swanson, J. Eckert, and J. Goldstone, J. Phys. Chem. **95**, 10103 (1991).

[5] P. W. Cooper, *Explosives Engineering*, chapter 2, 3, 4, Wiley-VCH, 1996.

[6] Gordon Research Conference on Energetic Materials, 2006.

[7] L. D. Landau and E. M. Lifshitz, *Statistical Physics*, chapter 5, Butterworth-Heinemann, 3rd edition, 1980.

[8] J. Moore and N. Spencer, *Encyclopedia of Chemical Physics and Physical Chemistry*, chapter 17, Taylor, 2001.

[9] E. Wilson, J. Decius, and P. Cross, *Molecular Vibrations: The Theory of Infrared and Raman Vibrational Spectra*, chapter 8, Dover, 1980.

[10]

[11] J. D. Jackson, *Classical Electrodynamics*, chapter 7, John Wiley and Sons, Inc., 1999.

[12] H. Ibach and H. Luth, *Solid-State Physics: An Introduction to Principles of Materials Science*, chapter 5, Springer, 3rd edition, 2003.

[13] D. C. Harris and M. D. Bertolucci, *Symmetry and Spectroscopy: An Introduction to Vibrational and Electronic Spectroscopy*, chapter 3, 5, Dover, 1989.

[14] H. Ibach and H. Luth, *Solid-State Physics: An Introduction to Principles of Materials Science*, chapter 6, pages 126–129, Springer, 3rd edition, 2003.

[15] Z. Huang, B. Chen, and G. Gao, J. Mol. Struct. , 87 (2005).

[16] M. F. Foltz, Propellants, Explosives, Pyrotechnics **18** (1993).

VITA

Graduate College
University of Nevada, Las Vegas

Brian F. Yulga

Bachelor of Science, Physics, 2004
University of Wisconsin – Stevens Point
Stevens Point, Wisconsin

Publications:
Pravica, M.; Yulga, B.; Liu, Z.; Tschauner, TO. *Phys. Rev. B*. 2007, *76*, 064102.
Pravica, M.; Yulga, B.; Tkachev, S.; Liu, Z. *J. Phys. Chem. A*. 2009, *113* (32), pp 9133-9137.

Thesis Title: Static High Pressure FT-IR Spectroscopic Studies of TATB

Thesis Committee:
Committee Chairperson: Dr. Michael Pravica, Ph.D.
Committee Member: Dr. Lon Spight, Ph.D.
Committee Member: Dr. Stephen Lepp, Ph.D.
Graduate Faculty Representative: Dr. Clemens Heske, Ph.D.